약학박사 학위논문

Application of microemulsion for enhancing topical skin absorption of 20(S)-protopanaxadiol and oral absorption of rebamipide

20(S)-protopanaxadiol의 국소 피부 흡수와 rebamipide의 경구 흡수 개선을 위한 마이크로에멀젼의 적용

2017년 8월

서울대학교 대학원

약학과 약제과학 전공

김 기 택

Application of microemulsion for enhancing topical skin absorption of 20(S)-protopanaxadiol and oral absorption of rebamipide

20(S)-protopanaxadiol의 국소 피부 흡수와 rebamipide의 경구 흡수 개선을 위한 마이크로에멀젼의 적용

지도교수 김 대 덕

이 논문을 약학박사학위논문으로 제출함

2017 년 8월

서울대학교 대학원

약학과 약제과학 전공

김 기 택

김기택의 박사학위논문을 인준함

2017 년 8월

위 원 장	정 석 재	(인)
부 위 원 장	이 우 인	(인)
위 원	맹 한 주	(인)
위 원	윤 인 수	(인)
위 원	김 대 덕	(인)

ABSTRACT

Application of microemulsion for enhancing topical skin absorption of 20(S)−protopanaxadiol and oral absorption of rebamipide

Ki Taek Kim

Department of Pharmaceutical Sciences

The Graduate School

Seoul National University

20(S)-protopanaxadiol (20S-PPD) is an aglycosylated metabolite of ginsenosides such as compound K and ginsenoside Rb1, and possesses a potent skin anti-aging activity. However, due to its low aqueous solubility and large molecular size, a suitable formulation strategy is required in order to enhance skin deposition of 20S-PPD by improving its solubility and skin permeability. Rebamipide (RBP) is a potent anti-ulcer and anti-oxidative agent, which belongs to biopharmaceutics classification system (BCS) class IV with a poor oral bioavailability of less than 10%. Thus, enhancing the systemic exposure of RBP may increase its pharmacological activities after oral administration. The objective of the study was to develop microemulsion (ME)-based systems for the topical skin delivery of 20S-PPD and for the oral delivery of RBP. 20S-PPD-loaded ME and

ME-based hydrogel (MEH) formulations were prepared and evaluated in terms of their particle size distribution, morphology, maximum loading capacity, viscosity, and pH value. Then, the *in vitro* and *in vivo* deposition or permeation profiles of 20S-PPD in the selected MEH formulation were studied using hairless mouse skin model and artificial skin model, Strat-M® membrane. A Carbopol-based MEH system of 20S-PPD was successfully prepared with a mean droplet size of 110 nm and polydispersity index of 0.436. The formulation was stable at least for 56 days, and its viscosity was high enough for its topical skin application. It significantly enhanced the *in vitro* and *in vivo* skin deposition of 20S-PPD with no influence on its systemic absorption in hairless mice. Notably, it was found that the rank of the tested formulaions in the order of decreasing deposition of 20S-PPD in *in vitro* Strat-M® membrane and *in vitro*/*in vivo* hairless mouse skin was same. For RBP-loaded ME, characterization study (*i.e.* maximum loading capacity, particle size distribution, and morphology), in vitro drug release study, in vivo pharmacokinetic study, and intestinal toxicity study were performed. Capmul MCM EP and Solutol HS15-based ME system of RBP had spherical nano-sized droplets with polydispersity index of 0.265 and neutral zeta potential. Moreover, the prepared ME significantly enhanced the dissolution and oral bioavailability of RBP with no discernible intestinal toxicity. Taken together, the ME-based systems developed in this study could serve as a potentially effective topical skin and oral delivery system for enhancing the absorption of poorly soluble compounds including 20S-PPD and RBP.

Keywords: 20(S)-protopanaxadiol (20S-PPD); rebamipide (RBP); microemulsion

(ME)-based systems; topical skin delivery; oral delivery; poorly soluble compound

Student Number: 2011-21702

Contents

ABSTRACT I

List of Tables VIII

List of Figures IX

Background 1

1.1. Fick's diffusion law 1

1.2. Microemulsion (ME)-based systems 3

1.3. Microemulsion (ME) systems for topical skin and oral delivery 5

Part I. Microemulsion-based hydrogels for enhancing epidermal/dermal deposition of topically administrated 20(S)-protopanaxadiol: *in vitro and in vivo* evaluation

1. Introduction 9

2. Materials and Methods 12

2.1. Materials 12

2.2. Animal 12

2.3. Solubility study 13

2.4. Construction of pseudo-ternary phase diagrams 14

2.5. Preparation of 20S-PPD-loaded ME and MEH formulations 14

2.6. Characterization of 20S-PPD-loaded ME and MEH formulations 15

2.6.1. Particle size and zeta potential 15

2.6.2. TEM 16

2.6.3. pH 16

2.6.4. Viscosity 16

2.6.5. Maximum loading capacity 17

2.7. *In vitro* skin deposition study: hairless mouse skin and Strat-M® membrane 17

2.8. *In vivo* skin deposition study 19

2.9. Stability study 20

2.10. LC-MS/MS analysis of 20S-PPD 20

2.11. Statistical analysis 22

3. Results 23

3.1. Preparation of 20S-PPD-loaded ME and MEH formulations 23

3.2. Characterization of 20S-PPD-loaded ME and MEH formulations 23

3.3. *In vitro* deposition of 20S-PPD in hairless mouse skin and Strat-M® membrane 25

3.4. *In vivo* skin deposition of 20S-PPD after topical application 26

3.5. Stability of 20S-PPD-loaded ME and MEH formulations 26

4. Discussion 28

5. Conclusion 34

Part II. Capmul MCM EP/Solutol HS 15-based microemulsion for enhanced oral bioavailability of rebamipide

1. Introduction 51

2. Materials and Methods 54

2.1. Materials 54

2.2. Animal 54

2.3. Solubility study 55

2.4. Construction of pseudo-ternary phase diagrams 55

2.5. Preparation of RBP-loaded MEs 56

2.6. Characterization of RBP-loaded MEs 56

2.6.1. Maximum loading capacity 57

2.6.2. Particle size and zeta potential 57

2.6.3. TEM 57

2.7. *In vitro* drug release study 58

2.8. *In vivo* pharmacokinetic study 58

2.9. *In vivo* intestinal toxicity study 59

2.10. HPLC-fluorescence analysis of RBP 59

2.11. Statistical analysis and data analysis 60

3. Results 62

3.1. Preparation of RBP-loaded MEs 62

3.2. Characterization of RBP-loaded MEs 62

3.3. *In vitro* release of RBP 63

3.4. *In vivo* plasma concentration profiles of RBP after oral administration at the dose of 5 mg/kg in rats 63

3.5. *In vivo* intestinal toxicity after oral administration at the dose of 5 mg/kg in rats.....64

4. Discussion.....65

5. Conclusion.....68

References.....80

국문초록.....91

Appendix.....94

List of Tables

Part I. Microemulsion-based hydrogels for enhancing epidermal/dermal deposition of topically administrated 20(S)-protopanaxadiol: *in vitro and in vivo* evaluation

Table 1 Solubility (mg/mL) of 20S-PPD in various vehicles.....35

Table 2 Weight compositions of ME formulations containing 0.1% (w/w) of 20S-PPD.....36

Table 3 Physicochemical properties of 20S-PPD-loaded ME and MEH formulations.....37

Table 4 Contents (% of initial loading dose) of 20S-PPD in the oil solution, P1, P5, and P5-H formulations stored at room temperature (RT) or 40°C on 0 (immediately after preparation), 7, 14, 28, and 56 days.....38

Part II. Capmul MCM EP/Solutol HS 15-based microemulsion for enhanced oral bioavailability of rebamipide

Table 1 Solubility (mg/mL) of RBP in various vehicles.....69

Table 2 Weight compositions of ME formulations containing 0.1% (w/w) of RBP 70

Table 3 Physicochemical properties of blank ME and RBP-loaded ME (R1).....71

Table 4 Pharmacokinetic parameters of RBP after the oral administration of the RBP suspension and R1 at a dose of 5 mg/kg to rats (n=4).....72

List of Figures

Part I. Microemulsion-based hydrogels for enhancing epidermal/dermal deposition of topically administrated 20(S)-protopanaxadiol: *in vitro and in vivo* evaluation

Figure 1 Chemical structure of 20(S)-protopanaxadiol (20S-PPD) 39

Figure 2 Pseudo-ternary phase diagrams of water, Capmul MCM EP (oil), and surfactant mixture (S_{mix}). The S_{mix} was the mixture of Labrasol and Tween 20 at 1:1, 2:1, and 3:1 ratio (w/w). Transparent MEs were formed in the clear region, and the other region represents turbid emulsions. The closed circle represents the compositions of ME formulations prepared with the three different S_{mix} ratios (1:1, 1:2, 1:3 for P1, P2, and P3, respectively) 40

Figure 3 Transmission electron microscopy (TEM) images and particle size distribution of 20S-PPD-loaded ME and MEH formulations. The scale bars represent 0.5 μm 41

Figure 4 *In vitro* deposition of 20S-PPD in the stratum corneum (SC) and epidermis/dermis of hairless mouse skin at 6 hr and that in Strat-M® membrane at 3 hr after the topical administration of P1, P2, and P3 at the concentration of 0.1% (w/w). The rectangular bars and their error bars represent the means and standard deviations, respectively (n = 3). The asterisk represents a value significantly different from that of the other groups, and the pound sign represents a significant difference between the two groups indicated (p < 0.05) 42

Figure 5 *In vitro* skin deposition of 20S-PPD in the stratum corneum (SC) and epidermis/dermis of hairless mouse skin at 6 hr and in Strat-M® membrane at 3 hr after the topical administration of P1, P4, and P5 at the concentration of 0.1% (w/w). The rectangular bars and their error bars represent the means and standard deviations, respectively (n = 3). The asterisk represents a value

significantly different from that of the other groups, and the pound sign represents a significant difference between the two groups indicated (p < 0.05) 43

Figure 6 *In vitro* deposition of 20S-PPD in Strat-M® membrane at 3 hr after the topical administration of suspension, oil solution, and P5-H at the 20S-PPD concentration of 0.1% (w/w). The rectangular bars and their error bars represent the means and standard deviations, respectively (n = 3). The asterisk represents a value significantly different from that of the other groups (p < 0.05).....44

Figure 7 *In vivo* skin deposition of 20S-PPD at 3, 6, and 12 hr in the stratum corneum (A) and epidermis/dermis (B) of hairless mouse skin after the topical administration of suspension, oil solution, and P5-H containing 0.1% (w/w) 20S-PPD at a dose of 25 mg/kg. The rectangular bars and their error bars represent the means and standard deviations, respectively (n = 3). The asterisk represents a value significantly different from that of the other groups, and the pound sign represents a significant difference between the two groups indicated (p < 0.05) 45

Figure 8 *In vivo* plasma concentration levels of 20S-PPD at 3, 6, and 12 hr after the topical administration of suspension, oil solution, and P5-H containing 0.1% (w/w) 20S-PPD at a dose of 25 mg/kg in hairless mice. The rectangular bars and their error bars represent the means and standard deviations, respectively (n = 3). 46

Figure 9 Correlation of the *in vitro* deposited 20S-PPD amounts at 3 hr in Strat-M® membrane with the *in vitro* deposited 20S-PPD amounts at 6 hr (A) and *in vivo* deposited 20S-PPD amounts at 3 hr (B), 6 hr (C), and 12 hr (D) in the epidermis/dermis of hairless mouse skin. The bullet symbols and their error bars represent the means and standard deviations, respectively (n = 3). The solid lines represent the fitted linear regression curves. 47

Figure 10 Particle size distribution of F1 and F5 stored at room temperature (RT) and 40℃ for 14, 28, and 56 days.....49

Part II. Capmul MCM EP/Solutol HS 15-based microemulsion for enhanced oral bioavailability of rebamipide

Figure 1 Chemical structure of rebamipide (RBP) 73

Figure 2 The solubility of RBP at various pH conditions 74

Figure 3 Pseudo-ternary phase diagrams of systems containing water, Capmul MCM EP (oil), and surfactant mixture (S_{mix}). The S_{mix} was the blend of Solutol HS 15 as surfactant and ethanol (a) or transcutol (b) as co-surfactant at 3:1 ratio (w/w). Another S_{mix} was the blend of Tween 80 as surfactant and ethanol (c) or transcutol (d) as co-surfactant at 5:3 ratio (w/w). Clear and transparent MEs were formed in the ME area, and other area represents turbid emulsion. The closed circles (●) represent the RBP MEs studied (R1, R2, R3, and R4) 75

Figure 4 Intensity distribution diagrams of mean diameters and TEM images of RBP formulation (a, blank R1; b, RBP-loaded R1). The scale bars represent 1 μm 76

Figure 5 Time profiles of *in vitro* drug release of RBP from suspension (●), R1 (○) in pH 1.2 buffer (a), pH 4.0 buffer (b), and pH 6.8 buffer (c) containing 0.2% SLS (Mean ± SD) 77

Figure 6 Time profiles of arterial plasma concentrations of RBP after oral administration of RBP suspension (●), R1 (○) at a dose of 5 mg/kg to rats (Mean ± SD, *n* = 4) 78

Figure 7 Representative histological sections of jejunal segments at 24 hr after oral administration of DW (a), blank R1 (b), RBP suspension (c), and R1 (d) to rats. The scale bars represent 500 μm 79

Background

1.1. Fick's diffusion law

In general, passive diffusion process is considered as main mechanism of absorption into the skin and gastro-intestinal (GI) membrane [1,2]. In this reason, the molecules which have low aqueous solubility would show limited absorption through the skin and GI membrane [3]. Absorption into the skin and GI membrane via passive diffusion mechanism can be described by Fick's laws [1,4].

$$J = \frac{dM}{S \cdot dt} \tag{1}$$

$$J = -D\frac{dC}{dx} = D\frac{C_1 - C_2}{h} \tag{2}$$

J is the flux (g/cm^2·sec) which means the rate of diffusion flows through unit area. M is the amount (g) of diffusant that penetrated the membrane after time t (sec). S is the area (cm^2) of membrane applied. D is the diffusion coefficient (cm^2/sec) of the diffusant. C_1 is the concentration (g/mL) of diffusant in the membrane at the donor side. C_2 is the concentration of diffusant in the membrane at the receptor side, and h is the thickness (cm) of membrane.

$$K = \frac{C_1}{C_d} = \frac{C_2}{C_r} \tag{3}$$

K is the partition coefficient of diffusant into membrane. C_d is the concentration of

diffusant in donor solution. C_r is the concentration of diffusant in receptor solution. The rate of diffusion (*dM/dt*) can be expressed as follows:

$$\frac{dM}{dt} = D \cdot S \cdot K \frac{C_d - C_r}{h} \quad (4)$$

$$P = \frac{D \cdot K}{h} \quad (5)$$

P is the permeability coefficient (cm/s). Assuming the sink condition at the receptor side, C_r is nearby almost 0. Therefore, the cumulative amount diffused (M) through membrane can be expressed as follows (Equation 6 and 7):

$$M = P \cdot S \cdot (C_d - C_r) \cdot t \quad (6)$$

$$= P \cdot S \cdot C_d \cdot t \quad (7)$$

As shown in the equation 6 or 7, M is proportional to P, S, and t. Also, as C_d increases, M will be increased. In oral delivery, the receptor side may be blood capillary which can be considered as sink condition. Thus, the absorption into GI membrane will be increased as the concentration of diffusant in its formulation after the oral administration (C_d). In topical skin delivery, the deposition into the epidermis and dermis of skin may be accumulated over time, which it may be non-sink condition. Nonetheless, the absorption and deposition into the skin will be increased as the concentration of diffusant in its formulation applied to the skin (C_d) increases by the rule of Fick's laws [4]. Therefore, solubilization of hydrophobic molecules can be the main approach for their enhanced absorption via

passive diffusion into the skin and GI membrane.

1.2. Microemulsion (ME)-based systems

Recent studies have suggested that modified formulations of poorly water-soluble agents such as solid dispersion, inclusion complexation, liposomes, and nanoparticles could enhance their solubility, thereby increasing bioavailability or absorption [5]. Among these strategies, microemulsion (ME)-based systems have been widely used for clinical and commercial products to overcome their own solubility problem [5].

ME is composed of oil, water, and surfactant mixture (S_{mix}) phase, which is isotropic, transparent and thermodynamically stable colloidal system with droplet sizes ranging from 10 to 200 nm [6,7]. MEs are clearly different from coarse emulsions that are cloudy in appearance (1 to 20 μm) and less stable than MEs [7]. In contrast to emulsions, MEs must need much more surfactant and, unlike emulsions, also co-surfactant which enable low interfacial tension in ME droplets [6]. The oil components of ME have usually been used with triglycerides (*i.e.* olive oil, soybean oil, and medium chain triglycerides), fatty acids (*i.e.* oleic acid and linoleic acid) or fatty acid esters (*i.e.* isopropyl myristate and isopropyl palmitate) [8]. In aqueous phase of ME, distilled water (DW) or buffer solution has been used. Natural surfactant including lecithin, non-ionic surfactant such as polysorbates (Tween 20 and Tween 80), sorbitane monooleate (Span 80), labrasol, and poloxamer or ionic surfactant including sodium lauryl sulfate and cetyl-trimethyl ammonium bromide has widely been used as surfactant phase of ME. The

co-surfactants of ME have usually been used with short- and medium-chain alcohols (*i.e.* ethanol and 1-butanol) or their derivatives (*i.e.* propylene glycol and transcutol) [8]. Among those phase in ME systems, hydrophobic molecules can be solubilized in the oil phase and/or adsorbed into the oil-water interface of ME, which allows higher loading capacity of the ME formulation, enhancing the driving force of their penetration through the membrane of skin or GI membrane [8,9]. By the ratio of water, oil and S_{mix} phase, the different structures of ME-based systems can be formed [8,10]. As the water phase in ME increase, the structure would be near to micelle. On the other hand, as the S_{mix} phase in ME increase, the structure would be presented bicontinuously or lamellarly, not spherically. Among the different MEs, oil in water (o/w) ME which can solubilize hydrophobic molecules can be formed when the water phase exists more than the oil phase and the proportion of S_{mix} phase is medium [10]. Although there are continuous diffusional processes and collisions at the interfaces of ME droplets, the equilibrium size and shape of the droplets are maintained [10].

To apply ME-based systems transdermally, topically, or orally, the acceptability of surfactants must be considered [8,10]. Because large amounts of a surfactant and a co-surfactant are required for ME systems, it might be cause intolerance like irritation, sensitization, and erythema [8]. Those side-effects can be minimized by a careful selection of the ME components. Among them, generally, non-ionic surfactants have been reported to have minimal toxicity compared with ionic surfactants, therefore, being more suitable for the use in ME-based systems [8,10]. Representatively, Tween 20 and Tween 80 have been widely used and accepted for transdermal and oral administration [8]. Labrasol (caprylocaproyl

macrogol-8 glycerides) and Solutol HS 15 (polyethylene glycol (15)-hydroxy-stearate), also have been investigated as surfactant in o/w ME [8]. Those surfactants were reported as biodegradable and only mildly irritating agents. To overcome the safety issues, the ME systems could be formulated without co-surfactant. However, these ME systems are more easily destabilized during storage [10]. Therefore, adequate amount of co-surfactant are needed for formation of stable ME with relatively low toxicity.

1.3. Microemulsion (ME) systems for topical skin and oral delivery

The ME-based systems has been widely applied for improvement of topical skin transport into and across skin layer, because some ingredients of ME formulation such as surfactants can serve as permeation enhancers to overcome barrier functions of skin [11,12]. ME applied topically was shown to enhance accumulation of quercetin as an anti-oxidant at the target site in the skin without increasing its systemic absorption [13]. In topical delivery of triptolide as anti-inflammatory agent, isopropyl myristate (oil phase) and Tween 80 (surfactant phase) based ME was developed and enhanced the skin deposition of triptolide [14]. Also, o/w MEs delivered ascorbyl palmitate to the skin significantly higher than its solution, thereby enhancing its efficacy as anti-oxidant [15]. In several researches, it was demonstrated that a combination of ME and phospholipids or phosphatidylcholines could improve topical skin delivery of drugs via the enhanced flexibility of ME droplets with skin layers [16,17]. However, the topical skin

application of ME in the clinical or commercial fields has been often hindered due to its low viscosity. Thus, ME-based hydrogels (MEHs) have attracted as an alternative topical skin delivery system to solve the problem of low viscosity of MEs [6,18]. In general, MEH with an appropriate viscosity and good biocompatibility can prolong the retention time on the skin and reduce the risk of skin irritation after its topical application [18,19]. Moreover, the mean droplet size, surface charge, and morphology of ME entrapped in the gel networks might be not significantly changed during gelation process compared to that of MEs [6,9]. MEs incorporated into carbopol gels were prepared and evaluated for topical delivery of terbinafine hydrochloride [20]. In another study, ME-based hydrogel for topical administration of fluconazole was developed [21]. Gelatin-containing ME-based gel using Tweem 85 and isopropyl myristate as surfactant was also investigated for skin delivery of sodium salicylate [22]. Soy bean phosphatidylcholine (lecithin)-containing ME-based gel has been investigated for skin delivery and skin irritation test was performed in humans, which showed a very low irricacy potential [23].

The ME-based systems offer several merits over conventional oral formulation, including enhanced absorption, improved pharmacological potency and negligible drug toxicity [24]. Unlike emlusion, MEs can be stable in aqueous media and even, in the gastro-intestinal fluids without emulsification by bile salts. Due to its nano-sized droplets and permeation-enhancing effect by surfactants, consequently, this systems leads to improved oral absorption of drugs [24]. Among ME-based systems, o/w MEs can significantly improve the oral bioavailability of hydrophobic drugs [10]. Curcumin, well-known as poorly water-soluble compound, was solubilized in o/w MEs, thereby its dissolution and *in vivo* oral absorption

being improved [25]. Furthermore, these o/w MEs can enhance the oral absorption of BCS class IV drugs which have a low solubility and a low permeability (i.e. docetaxel and paclitaxel) [10]. ME systems containing docetaxel was prepared and investigated for its solubilization effect and enhancement of *in vitro* dissolution and *in vivo* oral bioavailability [26]. Also, the oral absorption of paclitaxel was significantly enhanced by ME systems [27]. The developed MEs increased both the dissolution and permeability of paclitaxel. To overcome the stability of MEs and its large volume, self-micro emulsifying drug delivery system (SMEDDS) has been developed. SMEDDS is mixture of oils, surfactants, and co-surfactants which are self-emulsified in the gastro-intestinal fluid after the oral administration [24]. It also can improve the oral absorption of BCS class IV drugs. The drug release and oral bioavailability of simvastatin was improved via SMEDDS containing Carpryol 90, Cremophor EL, and Transcutol [28]. Neoral®, a SMEDDS of cyclosporin which contained oil solution of drug and surfactants, has been introduced to replace conventional crude emulsion of cyclosporine, Sandimmune® [29].

In summary, MEs as drug delivery systems improved the absorption of hydrophobic compounds into the skin or oral, which was attributed by their capacity of solubilization and permeation-enhancing effect.

Part I. Microemulsion-based hydrogels for enhancing epidermal/dermal deposition of topically administrated 20(S)-protopanaxadiol: *in vitro and in vivo* evaluation

1. Introduction

Among a number of active compounds in ginseng, ginsenosides are

known to be mainly responsible for diverse pharmacological effects of ginseng [30]. Among the various effect, ginsenoside F1 and Rb1 were reported to have anti-melanogenic activity in human skin and B16 cells, respectively [31,32]. More recently, a compound K-rich fraction prepared from ginseng was reported to have anti-photoaging activity by modulating several signaling pathways in α-MSH-treated B16F10 cells and UVB-irradiated NIH3T3 fibroblasts [33]. However, those studies were conducted by using classical formulations such as solutions and creams for the topical dermal application of ginsenosides. Considering a limited solubility and membrane permeability of ginsenosides mentioned above [34,35], further studies on suitable topical delivery systems are warranted to develop more effective cosmeceutical preparations containing ginsenosides.

20(S)-protopanaxadiol (20S-PPD, Fig. 1) is an agly-cosylated metabolite of ginsenosides such as compound K, Rb1, Rb3, Rg3, and Rh2 [36]. It possesses various pharmacological activities such as cardio-protective, antitumor, anti-inflammatory and antidepressant effects [36,37]. Notably, a recent study demonstrated that 20S-PPD presented markedly higher anti-wrinkle and skin-whitening effects compared with compound K and Rb1 in immortalized human keratinocytes and 3D-cultured human skin equivalent models, by the suppression of matrix metalloproteinases which are capable of degrading collagen and elastin in the epidermis and dermis of skin [38]. However, there also have been no studies about delivery systems on the topical skin delivery of 20S-PPD up to date. Moreover, due to the low aqueous solubility of 20S-PPD (< 50 ng/mL), as well as its relatively large molecular size (460.7 Da), its permeation through the stratum corneum and deposition in the epidermis and dermis parts of skin would be

restrictive based on the Fick's laws of diffusion [1,3]. Therefore, a suitable formulation strategy to improve the solubility and skin permeability of 20S-PPD is essential for its epidermal and dermal deposition enhancement. Moreover, to our best knowledge, there have been no studies which reported the topical application of 20S-PPD with nano-sized delivery systems including MEs and MEHs which have been considered to be appropriate for topical skin delivery. For these reasons, both MEs and MEHs were studied as delivery systems for the enhanced topical delivery of 20S-PPD in the present study.

Due to a limited availability of obtaining human skin and its high variability in lipid and protein compositions depending on bodyweights, genders, ages, diets, etc., hairless mouse skin has been widely regarded as a useful alternative to human skin on development of topical skin and transdermal formulations [39]. Previous studies have reported a good correlation of skin permeation profiles between human and hairless mouse skin due to the similarity of skin structures and lipid or protein compositions between them [40]. Also, in recent researches on topical skin delivery including cosmetic agents, the substitution for using animals in evaluation of skin absorption has been magnified. To substitute for animal skins for the evaluation of skin deposition or permeation, several artificial membranes were developed and have been studied [41,42]. Among them, Strat-M® membrane (Merck Millipore Co., Darmstadt, Germany), one of the commercially available, skin-mimic artificial membranes, has been recently introduced and widely used as non-animal based model [41]. Strat-M® membrane is composed of two layers of polyether sulfone which could represent the stratum corneum of skin and one layer of polyolefin which is more porous and diffusive, thereby could

represent the dermis of skin [42]. Due to these similarities, the membrane has been reported to have good-correlation in skin permeation profiles with human and animal skins [41,42]. However, to our best knowledge, little information is available regarding the correlation of skin deposition profiles between Strat-M membrane and animal skins. Therefore, in the present study, prepared ME and MEH formulations containing 20S-PPD were evaluated on its deposition by using hairless mouse skin and also, using Strat-M® membrane.

Finally, the objective of the present study is to investigate the feasibility of applying pharmaceutical drug delivery technology to the topical delivery of 20S-PPD by using MEs and MEHs. The 20S-PPD-loaded ME and MEH formulations were prepared by the construction of pseudo ternary phase diagram and characterized *in vitro* in terms of loading capacity, particle-size distribution, morphology, surface charge, viscosity, and long-term stability. Then, the *in vitro* and *in vivo* skin deposition properties of the prepared ME and MEH formulations were studied using hairless mice and Strat-M® membrane, a skin-mimic artificial membrane. Additionally, the correlation of skin deposition profiles of 20S-PPD between hairless mouse skin and Strat-M® membrane was investigated.

2. Materials and Methods

2.1. Materials

20(S)-protopanaxadiol (20S-PPD) (purity ≥ 98.0%) was purchased from Xian Plant Bio-Engineering Co., Ltd. (Shaanxi, China). Capmul MCM EP was gifted as a sample from ABITEC Co. (Columbus, OH, USA). Labrafac CC, Lauroglycol CC, labrasol (PEG-8 caprylic/capric glycerides) and Transcutol HP were gifted as samples from Gattefossé Co. (Saint Priest, Cedex, France). Tween 20, isopropyl myristate, Limonene, polyethylene glycol 400 (PEG400), sodium lauryl sulfate (SLS), soybean phosphatidyl choline (soy PC), xanthan gum, triethanolamine, and ketoprofen were purchased from Sigma-Aldrich Chemical Co. (St. Louis, MO, USA). Poloxamer 407 was obtained from BASF Co. (Ludwigshafen, Germany). Carbopol 941 was obtained from The Lubrizol Co. (Wickliffe, OH, USA). Phosphate buffered saline (PBS) was purchased from Lonza, Ltd. (Basel, Switzerland). HPLC grade methanol and acetonitrile were purchased from Thermo Fisher Scientific Co. (Pittsburgh, PA, USA). All other reagents were of analytical grade.

2.2. Animal

For *in vitro* and *in vivo* evaluation, male hairless mice (5 weeks age, 20–25 g) were used and obtained from Orient Bio Inc. (Sungnam, Korea). They were bred on sawdust and five mice were in each cage. They had free access to water and food before the studies. Room illumination was on an automatic cycle of 12 hr light/darkness, and room temperature was maintained at 25 ± 2°C. They were acclimatized to the presented conditions for at least one week prior to the experiments. Experimental protocols for the animals (Approval number: SNU-

111007-4-2) used in this study were reviewed by the Animal Care and Use Committee of the College of Pharmacy, Seoul National University and were in accordance with the National Institutes of Health's Guide for the Care and Use of Laboratory Animals (National Institutes of Health Publication Number 85-23, revised 1985).

2.3. Solubility study

The equilibrium solubility of 20S-PPD in various vehicles was determined by adding excess amount of them into 1 mL of each vehicle. The mixtures containing 20S-PPD were allowed to approach an equilibrium state in a vortex shaker (Vortex-Genie 2; Scientific Industries, Inc., Bohemia, NY, USA) with 50 rpm at 25°C for 72 hr. The samples were centrifuged at 16,000 x *g* for 5 min and the supernatant was filtrated with 0.20 μm syringe filter to remove the excess amount of 20S-PPD. Finally, the concentration of 20S-PPD in the filtrated solution was quantified by LC-MS/MS after appropriate dilution with methanol.

2.4. Construction of pseudo-ternary phase diagrams

Based on the solubility test of 20S-PPD (Table 1), Capmul MCM EP was selected as an oil phase, and Labrasol and Tween 20 were selected as a surfactant mixture (S_{mix}) phase for 20S-PPD-loaded ME formulations. The pseudo-ternary phase diagram studies were performed to find a clear and transparent ME

formulations. The surfactant and co-surfactant were mixed at different ratios to form the surfactant mixture (S_{mix}). Afterwards, the oil phase and the S_{mix} were mixed, where the ratios of oil to S_{mix} were varied as 9:1, 8:2, 7:3, 6:4, 5:5, 4:6, 3:7, 2:8, and 1:9 (w/w). Then, the water phase (distilled water, DW) was added drop-wise to each oil and S_{mix} mixture at room temperature with stirring to allow equilibration. After equilibrium, the mixtures were visually checked for transparency. The points from clear to turbid state were presented on the diagrams.

2.5. Preparation of 20S-PPD-loaded ME and MEH formulations

From the clear region of pseudo-ternary phase diagrams, three ME formulations (P1–P3) were selected for further evaluations (Table 2). For the preparation of MEs of 0.1% (w/w) 20S-PPD, exact amount of 20S-PPD was first added into Capmul MCM EP and vortex-mixed to dissolve 20S-PPD. Labrasol and Tween 20 mixtures were subsequently added to the 20S-PPD oil solution under gentle stirring at room temperature. Then, DW was added dropwise into the above mixture at the same condition. In order to investigate the synergic effect of co-surfactants (*i.e.*, Transcutol HP and Soy PC), they were added into the S_{mix}, after which 20S-PPD in Capmul MCM EP and DW were added as described above (P4 and P5, Table 2).

For the preparation of MEH, different hydrophilic polymers were used. An appropriate amount of hydrophilic polymers such as xanthan gum or poloxamer 407 was added in the 20S-PPD-loaded ME and swelled overnight under magnetic stirring. After sonication for 10 min, the semisolid hydrogel was obtained. The final

concentration of xanthan gum and poloxamer 407 in each 20S-PPD-loaded MEH was 1.0% and 15.0% (w/w), respectively. For carbopol hydrogel, carbopol 941 was dispersed in the 20S-PPD-loaed ME and swelled overnight under magnetic stirring. Then, appropriated amount of triethanolamine (TEA) was added to neutralize the pH value until a semisolid hydrogel was obtained. The final concentration of carbopol 941 in 20S-PPD-loaded MEH was 1.0% (w/w). Selection of appropriate MEH for topical skin delivery among the various MEH formulations as mentioned above was performed by the observation of their visual appearance and determination of their viscosity.

2.6. Characterization of 20S-PPD-loaded ME and MEH formulations

2.6.1. Particle size and zeta potential

The mean particle size, polydispersity index, intensity distribution of particle size, and zeta potential of 20S-PPD-loaded MEs were measured in triplicate by an electrophoretic light-scattering (ELS) spectrophotometer (ELS 8000, Otsuka Electronics Co. Ltd., Tokyo, Japan). The prepared MEs were transferred to a quartz cuvette before the measurement. All measurements were performed at 25°C in triplicate.

2.6.2. TEM

The particle morphologies of 20S-PPD-loaded ME and MEH formulations were observed by an energy-filtering transmission electron microscopy (TEM) (LIBRA 120, Carl Zeiss, Germany) at 80 kV. The samples were placed on a carbon-coated copper grid and negatively stained by 2% phosphotungstic acid followed by drying at room temperature before the operations.

2.6.3. pH

The pH value of 20S-PPD-loaded ME and MEH formulations was evaluated by using a pH meter (OrionTM 3-Star Benchtop; Thermo Fisher Scientific Co.) at 25°C in triplicate after calibration with standard pH buffer solutions at the pH range of 4.0 to 10.0.

2.6.4. Viscosity

The viscosity of 20S-PPD-loaded ME and MEH formulations was evaluated using rotational viscosity measurement device coupled with concentric cylinder (LV1) at 25°C (Brookfield viscometer LVDVE; Brookfield Engineering Laboratories, Inc., Middleboro, MA, USA).

2.6.5. Maximum loading capacity

To confirm the maximum 20S-PPD-loading capacity of ME and MEH formulations, excess 20S-PPD was added into the mixture of oil and S_{mix}, after which the 20S-PPD-loaded MEs or MEH were prepared as the same method before. Then, excess 20S-PPD which was not included into the droplets of ME was removed by centrifugation for 5.0 min at 16,000 x *g*. The supernatant was injected into LC-MS/MS for analysis of 20S-PPD after adequate dilution with methanol.

2.7. In vitro skin deposition study: hairless mouse skin and Strat-M® membrane

Evaluation of *in vitro* deposition of 20S-PPD into hairless mouse skin was carried out by using Keshary-Chien diffusion cells at 32°C, which have 1.77 cm^2 of the surface area for diffusion. After sacrificing the hairless mice by cervical dislocation, the dorsal skin was cut to appropriated size and the subcutaneous fat was removed. Then, they were fixed between the donor and receptor cells, laying the stratum corneum toward the donor cells. The receptor cells were filled with PBS containing 1.0 w/v% SLS (13.0 mL). Afterwards, various 20S-PPD loaded MEs (P1 to P5) were applied into the donor cell and sealed with parafilm to avoid evaporation of samples. The skin was removed from the diffusion cells at 6 hr after applying samples and washed out with methanol. In order to determine the amount of 20S-PPD in stratum corneum, tape stripping method was used [39]. Cellophane adhesive tape (CuDerm corporation, Dallas, TX, USA) was applied three times on

the stratum corneum of the skin and the tapes of each time samples were separately collected into the 2.0 mL tube. The skin samples after removing the stratum corneum (*i.e.*, epidermis and dermis) were chopped and collected into a mortar. The chopped samples were ground to powder using a pestle after adding liquid nitrogen. The skin powders were collected by Cellophane adhesive tape, and were transferred into the 2.0 mL tube. For extraction of 20S-PPD from the tapes, methanol (1.5 mL) was added and the tube was shaken for 3 hr, followed by centrifugation for 5.0 min at 16000 *g*.

Evaluation of *in vitro* deposition of 20S-PPD into Strat-M® membrane was carried out by using the same diffusion cell. Strat-M® membrane which has a 2.5 cm of diameter was fixed between the donor and receptor cells, laying the shiny side toward the donor cells. The receptor cells were filled with the same media as described above. Then, 20S-PPD in various vehicles (0.1%, w/w), *i.e.*, MEs (P1 to P5), MEH (P5-H), suspension (DW and propylene glycol mixture; 9:1 w/w), and oil (Capmul MCM EP) solution, was applied into the donor cell and sealed with parafilm to avoid evaporation of samples. The Strat-M® membranes were removed from the diffusion cells at 3 hr after applying samples and washed out with methanol. Then, they were put into the 2.0 mL tube and added with the mixture of acetone and methanol (70:30 v/v%, 1.5 mL). For extraction of 20S-PPD from the Strat-M® membrane, the tube was shaken for 3 hr, followed by centrifugation for 5.0 min at 16000 *g*. Then, an 1.0 mL aliquot of the supernatant was evaporated by a gentle nitrogen gas stream at 30°C and reconstituted with 0.5 mL of methanol. Finally, the amount of 20S-PPD in the stratum corneum and epidermis/dermis of hairless mouse skin at 6 hr and in Strat-M® membrane at 3 hr was analyzed using

LC-MS/MS.

2.8. In vivo skin deposition study

Evaluation of *in vivo* skin deposition and permeation of 20S-PPD was carried out using a male hairless mouse as animal model. The mouse was slightly anesthetized with ether before the experiment and fixed laying the dorsal part upward. For applying suspension (DW and propylene glycol mixture; 9:1 w/w) and oil (Capmul MCM EP) solution, a specially designed cylinder-type chamber which has a diffusion area of 0.79 cm2 was put on the dorsal skin of mice and fixed with surgical glue (Vet bond®, 3M Co., St. Paul, MN, USA). After recovering from anesthesia, suspension or oil solution containing 0.1 % (w/w) of 20S-PPD was applied into the chamber for topical administration of 20S-PPD. Also, 20S-PPD loaded MEH (P5-H) was applied on the same area of dorsal part by hand-rubbing. All formulation was administrated on the skin at a dose of 25 mg/kg. Before the sacrificing at 3, 6, and 12 hr, about 300 μL aliquot of blood sample was collected for evaluation of permeated 20S-PPD through the skin. Plasma samples were obtained by centrifugation for 5.0 min at 16000 *g* and stored at –20°C until LC-MS/MS analysis. After blood sampling from the hairless mice, they were sacrificed by cervical dislocation. Then, the skin samples were pretreated as described in the *in vitro* skin deposition study to determine the deposited 20S-PPD into the skin by using LC-MS/MS.

2.9. Stability study

The stability of 20S-PPD in various formulations at room temperature and 40°C for 7, 14, 28, and 56 days was evaluated by comparing 20S-PPD content and change of particle size distribution. Briefly, oil solution, 20S-PPD loaded MEs (P1 and P5) and MEH (P5-H) containing 0.1 % (w/w) of 20S-PPD were prepared and stored on the above conditions. At 0 (initial state), 7, 14, 28, and 56 days, mean particle size distribution of the samples was measured by the ELS spectrophotometer. For the determination of 20S-PPD content, the samples were centrifuged for 5.0 min at 16000 *g*, and then the supernatant was injected into LC-MS/MS after adequate dilution with methanol.

2.10. LC-MS/MS analysis of 20S-PPD

The amount of 20S-PPD was determined by LC-MS/MS analysis as described previously [37]. The samples were injected into an Agilent LC-MS/MS system (Santa Clara, CA, USA) equipped with an Agilent Technologies 1260 Infinity HPLC system and Agilent Technologies 6430 Triple Quad LC-MS system. The samples were injected through Hypersil BDS C18 column (50 mm×4.6 mm, 5 μm; Thermo Fisher Scientific Co.). The mobile phase was 93% acetonitrile and 7% water containing 0.2% formic acid (v/v). The flow rate was 0.37 mL/min. Determination of 20S-20S-PPD was conducted in the multiple reaction monitoring mode with positive electrospray ionization (ESI). The gas temperature, gas flow, nebulizer pressure, and capillary voltage were 120°C, 9 L/min, 25 psi, and 6000 V,

respectively. The m/z value of precursor to product ion, fragment voltage, collision energy, and cell accelerator voltage for 20S-PPD were 461.4 to 425.5, 111 V, 4 eV, and 1 V, respectively. The analytical data were processed using the MassHunter Workstation Software Quantitative Analysis (vB.05.00; Agilent Technologies). The retention time of 20S-PPD was 1.09 min. The calibration standard samples were prepared by serial dilution with methanol, thereby yielding final concentration range of 2.0–1000 ng/mL. The response of detector was linear in the concentration range and the mean correlation coefficient (r^2) for the calibration curve was over 0.999. The signal to noise ratio on the lower limit of quantification (LLOQ = 2.0 ng/mL) was higher than 5.0 and there was no interference from any other substances.

Plasma samples containing 20S-PPD were allowed to thaw at room temperature for analysis. A 100 μL aliquot of each sample was deproteinized with a 1 mL aliquot of methanol containing 500 ng/mL ketoprofen as an internal standard (IS). After vortex-mixing for 5 min, followed by centrifugation at 16000 *g* for 5 min, a 900 μL aliquot of the supernatant was transferred and evaporated by nitrogen gas at 40°C. Then, the film was reconstituted with a 100 μL aliquot of methanol. After vortex-mixing for 5 min, followed by centrifugation at 16000 *g* for 5 min, the supernatant was injected into an Agilent LC-MS/MS system with the same column and MS/MS conditions. The mobile phase was 88% acetonitrile and 12% water containing 0.2% formic acid (v/v). The flow rate was 0.40 mL/min. The *m/z* value of precursor to product ion, fragment voltage, collision energy, and cell accelerator voltage for 20S-PPD were the same as above. Those parameter for IS were 255.1 to 209.1, 110 V, 11 eV, 1 V, respectively. The retention time of 20S-

PPD and IS was 1.17 and 0.51 min, respectively. The calibration standard samples were prepared by spiking working standard into the blank plasma, thereby yielding final concentration range of 2.0–1000 ng/mL. The response of detector was linear in the concentration range and the mean correlation coefficient (r^2) for the calibration curve was over 0.999. The signal to noise ratio at the LLOQ (2.0 ng/mL) was higher than 5.0.

2.11. Statistical analysis

All experiments in this study were performed at least three times, and the data are presented as mean ± standard deviation (SD). Statistical analyses were carried out using the two-tailed t-test or analysis of variance (ANOVA) with *post-hoc* test (IBM SPSS Statistics software, version 21.0; IBM Corp, Armonk, NY, USA), and $p < 0.05$ was considered significantly different.

3. Results

3.1. Preparation of 20S-PPD-loaded ME and MEH formulations

Due to a low aqueous solubility of 20S-PPD in DW (36.8 ng/mL), various oils and surfactants were tested to select suitable vehicles for 20S-PPD. The rank of the tested compounds in the order of decreasing solubility of 20S-PPD was as follows: Capmul MCM EP > Lauroglycol CC > Labrafac CC as oils;

Labrasol > Tween 20 > isopropyl myristate > limonene > PEG 400 as surfactants (Table 1). The pseudo-ternary phase diagrams consisting of water (DW), oil (Capmul MCM EP), and S_{mix} are shown in Fig. 2. The S_{mix} was the mixture of Labrasol and Tween 20 at three different ratios (1:1, 2:1, and 3:1, w/w). As shown in Fig. 2, the formation of clear and transparent ME was observed in constructing the pseudo-ternary phase diagrams with different S_{mix} ratios. Three ME formulations were selected within the clear and transparent area of MEs prepared with the three different S_{mix} ratios, *i.e.* P1, P2, and P3 (Table 2). Additionally, Transcutol HP and soy PC were employed as co-surfactants in the ME formulations P4 and P5 (Table 2). Then, MEH formulations were prepared by the addition of gelling agents, such as xanthan gum, Poloxamer 407, or Carbopol 941, into P5.

3.2. Characterization of 20S-PPD-loaded ME and MEH formulations

The compositions of 20S-PPD-loaded ME formulations are listed in Table 2. Physicochemical properties including droplet size, polydispersity index, zeta potential of 20S-PPD-loaded MEs are presented in Table 3. The mean droplet sizes of the prepared ME formulations (P1 to P3) ranged from 69.1 nm to 99.6 nm, and P1 had the smallest particle size. When Transcutol HP and soy PC were added as co-surfactants in P1, the mean droplet size slightly (not significantly) increased up to 106 and 110 nm in P4 and P5, respectively. Surface charge of droplets was observed to near neutral in all the 20S-PPD-loaded ME formulations tested. Particle size distributions and TEM images of P1 and P5 showed that spherical and

nano-sized particles with a narrow-to-moderate size distribution were observed in 20S-PPD-loaded MEs (Fig. 3).

MEH formulations were prepared by the addition of xanthan gum, Poloxamer 407, or Carbopol 941, into F5. When adding xanthan gum, a turbid and unclear formulation was observed. The rank of the viscosity of MEHs was as follows: Carbopol-based MEH (29400 mPa·s) > xanthan gum-based MEH (8420 mPa·s) > Poloxamer-based MEH (657 mPa·s). This result was consistent with the fluidity of MEHs observed in a horizontal position. Only Carbopol-based MEH was not flew down in a horizontal position. As shown in Fig. 3, it was confirmed by TEM picture that spherical droplets derived from P5 were located in the Carbopol gel (P5-H), and their droplet sizes looked similar to those of P5. The pH, viscosity, and maximum loading capacity values of the ME and MEH formulations are listed in Table 3. The pH value of P5-H (6.91) was close to neutral than those of other MEs (5.33 to 5.55). Besides, the viscosity of P5-H (29400 mPa·s) was much higher than in other MEs (9.33 to 11.2 mPa·s). There were no significant differences in maximum loading capacity among all the ME and MEH formulations tested, ranging from 3.56 to 3.94 mg/mL.

3.3. In vitro deposition of 20S-PPD in hairless mouse skin and Strat-M® membrane

Fig. 4 presents *in vitro* deposition of 20S-PPD at 6 hr in hairless mouse skin and at 3 hr in Strat-M® membrane after the topical application of P1, P2, and P3. The deposited amount of 20S-PPD at 6 hr in epidermis/dermis of hairless

mouse skin was the highest in P1 ($p < 0.01$), while there was no significant difference on the deposition of 20S-PPD in the SC among the three ME formulations tested. Moreover, the 20S-PPD deposition at 3 hr in Strat-M® membrane was higher in P1 than in P3 ($p < 0.05$). Fig. 5 shows the effect of co-surfactants (Transcutol HP and soy PC) added in the ME formulation P1. Notably, the deposited amounts of 20S-PPD at 6 hr in the epidermis/dermis of hairless mouse skin were significantly higher in P4 and P5 than in P1 ($p < 0.05$), while there was no significant difference on the deposition of 20S-PPD in the SC among the three ME formulations tested. Moreover, the 20S-PPD deposition at 3 hr in Strat-M® membrane was the highest in P5 ($p < 0.01$). Fig. 6 presents *in vitro* deposition of 20S-PPD at 3 hr in Strat-M® membrane after the topical application of suspension, oil solution, and P5-H formulations. The deposited amount of 20S-PPD was the highest in P5-H ($p < 0.001$), followed by oil solution and suspension group.

3.4. In vivo skin deposition of 20S-PPD after topical application

Figs. 7 and 8 present the *in vivo* skin deposition profiles and plasma concentration of 20S-PPD, respectively at 3, 6, and 12 hr after the topical administration of suspension, oil solution, and P5-H formulations in hairless mice. *In vivo* skin deposition and plasma concentration of 20S-PPD tended to increase over time in all the three formulations tested. The deposited amounts of 20S-PPD in the SC at 3 and 6 hr and in the epidermis/dermis at 3, 6, and 12 hr were significantly higher in P5-H than in the two control formulations ($p < 0.01$; Fig. 7).

However, there were no significant differences in the plasma concentrations of 20S-PPD permeated at 6 and 12 hr among all the formulations tested.

3.5. Stability of 20S-PPD-loaded ME and MEH formulations

Stability of 20S-PPD in oil solution, P1, P5, and P5-H at room temperature and 40°C for 56 days was evaluated in terms of phase separation/aggregation, particle size distribution, and drug content (Fig. 10 and Table 4). As a result, no aggregates were observed in the oil solution, P5, and P5-H formulations and their transparency also maintained through 56 days. However, the aggregates were observed in P1 at both temperatures on the 14th, 28th, and 56th day after preparation. Correspondently, these aggregates over 1.0 μm of particle size were observed on the particle size distribution of P1 and those portions in P1 droplets increased through 56 days (Fig. 10). Moreover, the 20S-PPD contents of oil solution, P5 and P5-H remained nearly to 100% at both temperatures for 56 days, while those of P1 were significantly reduced to 67.1% and 68.5% at room temperature and 40°C, respectively (Table 4).

4. Discussion

The present study provided novel data on the development of ME or MEH formulations for the topical delivery of 20S-PPD in order to enhance its absorption into the skin. To prepare ME systems for 20S-PPD, Capmul MCM EP was selected as an oil phase due to its higher ability to solubilize 20S-PPD as compared to the other oils tested (Table 1). Labrasol and Tween 20 were selected as constituents of S_{mix} phase, due to their higher ability to solubilize 20S-PPD as compared to the other surfactants tested (Table 1). The selected surfactants with high hydrophilic-lipophilic balance (HLB) values, *i.e.* 14.0 for Labrasol and 16.7 for Tween 20, are generally considered as emulsifiers suitable for the formation of

oil-in-water MEs [8]. In the pseudo-ternary phase diagram shown in Fig. 2, the three ME formulations (P1–P3) with different Labrasol-to-Tween20 ratios were selected based on the principle of high water portion and low S_{mix} portion within the transparent ME region [43]. Additionally, Transcutol HP (HLB = 4.2) and soy PC (HLB = 4.5) were employed as co-surfactants in the ME formulations F4 and F5 (Table 2) [44]. The combinations of high-HLB surfactants (*i.e.* Labrasol and Tween 20) and these low to medium-HLB co-surfactants are known to facilitate the formation of a stable ME [8,45]. Moreover, soy PC can increase the flexibility of oil-water interface, thereby enhancing physical stability of ME system [46,47]. The maximum loading capacity of 20S-PPD in all the ME formulations tested were above 3 mg/mL, which was markedly higher in comparison with the aqueous solubility of 20S-PPD in DW (36.8 ng/mL, Table 1). Based on this maximum loading capacity, the loading content of 20S-PPD in the ME formulations was set as 0.1% (w/w) for further studies in order to prevent aggregation and precipitation in ME system.

To prepare the MEH system, hydrophilic polymers such as xanthan gum, Poloxamer 407, and Carbopol 941 were employed as gelling agents in this study. However, the addition of xanthan gum to the ME formulations resulted in an instantaneous aggregate formation and considerably increased turbidity, probably due to an increase in oil-water interfacial tension caused by xanthan gum [48]. Moreover, the viscosities of poloxamer 407-based MEH formulations (657 mPa·s at room temperature and 2840 mPa·s at 32°C) were much lower than 20000 mPa·s that is generally considered suitable for topical dermal application [6,49]. Carbopol has been widely regarded as an useful component of drug delivery gel systems for

dermal, ocular, buccal, nasal, and rectal applications [50]. Due to the rheological properties of Carbopol gels such as remarkable temperature stability, long relaxation time, and low thixotropy, they have been considered as appropriate delivery systems for topical delivery systems requiring prolonged drug residence time with enhanced skin retention [51]. In our present study, the prepared MEH formulation containing 1.0% (w/w) Carbopol 941 and 2.0% (w/w) triethanolamine (P5-H) was transparent in appearance and exhibited an appropriate viscosity (29400 mPa·s) for topical dermal application.

The physicochemical properties of the ME or MEH formulations containing 20S-PPD were characterized as presented in Table 3. The mean droplet sizes of the 20S-PPD-loaded ME formulations significantly increased as the Labrasol-to-Tween 20 ratios increased (P1: 69.1 nm → P2: 79.1 nm → P3: 99.6 nm). The mean droplet sizes were further increased by the addition of co-surfactants (Transcutol HP and soy PC) into the P1 formulation and resultant increases in oil-to-water ratios (P4: 106 nm; P5: 110 nm). Notably, TEM images showed that the droplet sizes of P5 seemed to be comparable to those of P5-H (Fig. 3). This result is consistent with a previous study which reported no significant influence of Carbopol on the size and morphology of ME droplets [6,9]. The surface charges of droplets in all the formulations prepared were near neutral (Table 3), probably because they consisted of non-ionic surfactants and oil. This may reduce the risk of irritations on the skin or GI tract that can occur more often in topical or oral administration of charged ME formulations containing ionic surfactants [52]. The mean pH values of all the 20S-PPD-loaded ME and MEH formulations ranged from 5.33 to 6.91, which are comparable to a pH value of

normal human skin (5.5–6.5) [53]. The viscosities of ME formulations were markedly enhanced by the addition of Carbopol 941, which would be more appropriate for topical administration [9]. In the long-term stability test, P1 was observed to be stable for 7 days but unstable on 14th day and thereafter, while P5 and P5-H were stable through 56 days (Fig. 10 and Table 4). This may be attributable to the addition of co-surfactants (Transcutol HP and soy PC) in F5 and F5-H, thereby preventing the aggregation or precipitation of poorly soluble ingredients such as 20S-PPD.

Owing to a limited availability of human skin and its high variability in lipid and protein compositions depending on bodyweights, genders, ages, and diets, hairless mouse skin has been widely regarded as a useful alternative to human skin [39]. Previous studies have demonstrated a good correlation of skin permeation profiles between human and hairless mouse skin [40]. Based on these previous researches, hairless mice were regarded as a suitable animal model for alternative to the human skin in evaluation of deposition and permeation of 20S-PPD into the skin. Besides, Strat-M® membrane is a synthetic and non-animal-based model that is predictive of diffusion characteristics in human skin [41]. Due to its similarities as mentioned on the introduction, the membrane has been reported on its good-correlation of skin permeation profiles with human and animal skins [41,42]. Thus, Strat-M® membrane was also used in evaluation of deposition and permeation of 20S-PPD. Among P1, P2, and P3, the deposited amounts of 20S-PPD in both the epidermis/dermis of hairless mouse skin and Strat-M® membrane were the highest in P1. Previous studies reported that the skin permeation and deposition of ME or MEH systems were enhanced as their droplet sizes decreased [54,55]. Thus, it

appeared that the smaller droplet size of P1 than P2 and P3 (Table 3) may be responsible for the enhanced deposition of 20S-PPD in the epidermis/dermis of hairless mouse skin and Strat-M® membrane (Fig. 4), but further investigation is required to understand the exact mechanism(s). Notably, the incorporation of Transcutol as a co-surfactant into P1 significantly enhanced the deposited amount of 20S-PPD in both the epidermis/dermis of hairless mouse skin and Strat-M® membrane (P4 in Fig. 5). Moreover, the incorporation of soy PC as an additional co-surfactant into P4 further enhanced the deposition 20S-PPD in Strat-M® membrane (P5 in Fig. 5). Transcutol can act as a skin permeation enhancer by interacting with hydrophilic moieties of skin lipids and proteins [56]. Soy-PC, the main component of cell membranes, can readily fuse with the stratum corneum and increase its fluidity, thereby exerting skin permeation-enhancing effect [47,57]. Thus, it is reasonable that the enhancement of skin deposition of 20S-PPD observed in P4 and P5 may be attributed to the permeation-enhancing activity of co-surfactant added. Based on the results shown in Figs. 4 and 5, P5 were selected for further studies on the development of MEH formulation. The *in vitro* deposition of 20S-PPD after applying P5-based hydrogels (P5-H) together with suspension and oil solution formulations (serving as control groups) containing 20S-PPD (0.1%, w/w) was evaluated using Strat-M® membrane (Fig. 6). The deposited amount of 20S-PPD was significantly higher in P5-H than in the two control groups. Notably, as shown in Figs. 5 and 6, the Strat-M® membrane deposition of 20S-PPD in P5-H (157±10 ng/cm^2) was significantly lower than that in P5 (266 ± 31 ng/cm^2). Although the exact mechanism is unclear, a viscous gel network could have retarded the release of 20S-PPD from P5-H, resulting in the reduced

deposition of 20S-PPD. The *in vivo* skin deposition of 20S-PPD was evaluated after the topical administration of suspension, oil solution, and P5-H containing 20S-PPD (0.1%, w/w) at a dose of 25 mg/kg to hairless mice (Fig. 7). At all the time points studied, the extents of *in vivo* epidermal/dermal 20S-PPD deposition were in the following order: suspension < oil solution < P5-H, which presented a similar tendency to the *in vitro* 20S-PPD deposition in Strat-M® membrane (Fig. 6).

Recently, it was demonstrated that 20S-PPD showed its anti-wrinkle and skin-whitening effects at a concentration range from 250 nM to 1000 nM [38]. Assuming that the thickness of epidermis/dermis layer of male hairless mouse skin is 510 μm [58], the epidermal/dermal concentrations of 20S-PPD can be calculated from its *in vivo* deposited amounts. As a result, the calculated epidermal/dermal concentration values at all the time points were as follows: 200–274 nM in suspension group, 663–2180 nM in oil solution group, and 1490–3670 nM in P5-H group. In general, drug permeability in human skin tends to be lower by several folds than that in mouse skin [39]. Thus, it can be supposed that the suspension and oil solution formulations cannot provide a sufficient epidermal/dermal 20S-PPD concentration level after the topical application, which emphasizes potential merits of the MEH formulation (P5-H) developed in this study. Furthermore, the plasma concentration of 20S-PPD after the topical administration of P5-H were negligibly low and comparable to those of the control (oil solution) group (Fig. 8), indicating that our newly-developed MEH formulation (P5-H) does not affect the systemic absorption of 20S-PPD administered topically.

In the present study, Strat-M® membrane, as well as hairless mouse skin, was used in *in vitro* deposition studies of 20S-PPD. However, to our best

knowledge, little information is available regarding the correlation of skin deposition profiles of drugs between Strat-M membrane and hairless mouse skin. As shown in Fig. 9, good linear correlations (correlation coefficient r^2 = 0.929–0.947) between *in vitro* 20S-PPD deposition in Strat-M membrane and both *in vitro*/*in vivo* 20S-PPD deposition in hairless mice were found by linear regression analysis of skin deposition data for all the formulations studied. Notably, the slopes of all linear regression was higher than 1.0 (1.73 to 4.37, Fig. 9), which means the deposition of 20S-PPD into the Strat-M® membrane was higher than that in the epidermis/dermis of hairless mouse skin. It may be attributed to the relatively thin thickness (300 μm) of Strat-M® membrane compared to that of hairless mouse skin (> 500 μm) [41,58].

5. Conclusion

In the present study, the Carbopol-based MEH formulations were prepared for the topical delivery of a potential skin anti-aging agent, 20S-PPD. The formulations successfully enhanced the solubility, long-term stability, *in vitro*/*in vivo* skin deposition of 20S-PPD with no influence on its systemic absorption in mice. Notably, it was found that Strat-M® membrane provided skin deposition data well-correlated to those obtained from the present *in vitro*/*in vivo* mouse skin studies on the deposition of 20S-PPD. To our best knowledge, our results are the first reported data regarding the development of 20S-PPD-loaded ME/MEH formulations and their deposition profiles in hairless mouse skin and Strat-M® membrane. Taken together, the ME-based systems developed in this study could serve as a potentially effective topical skin delivery system for poorly soluble

ginsenosides including 20S-PPD.

Table 1 Solubility (mg/mL) of 20S-PPD in various vehicles.

Phase	Vehicles	Solubility
Water	DW	36.8 ± 4.83 (ng/mL)
Oil	Capmul MCM EP	10.6 ± 1.44
	Lauroglycol CC	6.87 ± 0.380
	Labrafac CC	3.80 ± 0.820
Surfactant	LAS [a]	8.63 ± 1.78
	Tween 20	5.37 ± 0.887
	Isopropyl myristate	2.53 ± 0.734

Limonene	1.54 ± 0.258
PEG 400	0.0152 ± 0.00487

[a] PEG-8 caprylic/capric glycerides.

Table 2 Weight compositions of ME formulations containing 0.1% (w/w) of 20S-PPD.

	Water	**Oil**	**Surfactant**		**Co-surfactant**	
	DW	Capmul MCM EP	Labrasol	Tween 20	Transcutol	Soy PC
F1	47.5	17.5	17.5	17.5		
F2	47.5	17.5	23.3	11.7		
F3	47.5	17.5	26.2	8.8		
F4	42.5	17.5	17.5	17.5	5.0	
F5	41.5	17.5	17.5	17.5	5.0	1.0

Table 3 Physicochemical properties of 20S-PPD-loaded ME and MEH formulations.

Parameters	**Droplet size** (nm)	**PDI** [c]	**Zeta potential** (mV)	**pH**	**Viscosity** (mPa·s)	**Maximal loading capacity** (mg/mL)
P1	69.1 ± 2.56	0.331 ± 0.006	- 0.353 ± 0.769	5.33 ± 0.257	10.3 ± 0.211	3.28 ± 0.243
P2	79.7 ± 1.80	0.254 ± 0.030	- 0.590 ± 1.13	5.41 ± 0.181	9.87 ± 0.493	3.79 ± 0.334
P3	99.6 ± 2.18	0.306 ± 0.028	- 0.740 ± 1.05	5.38 ± 0.149	9.33 ± 0.785	3.94 ± 0.159
P4	106 ± 1.10	0.347 ± 0.053	- 0.170 ± 0.452	5.45 ± 0.248	10.4 ± 0.191	3.63 ± 0.478
P5	110 ± 7.47	0.436 ± 0.019	- 1.08 ± 0.217	5.55 ± 0.314	11.2 ± 0.339	3.72 ± 0.562
P5-H	-	-	-	6.91 ± 0.249	29400 ± 882	3.56 ± 0.529

[c] Polydispersity index.

Table 4 Contents (% of initial loading dose) of 20S-PPD in the oil solution, P1, P5, and P5-H formulations stored at room temperature (RT) or 40°C on 0 (immediately after preparation), 7, 14, 28, and 56 days.

Time	Oil solution		P1		P5		P5-H	
	RT	40°C	RT	40°C	RT	40°C	RT	40°C
0 day (Initial)	98.4 ± 3.54	99.1 ± 3.26	98.4 ± 1.69	100 ± 4.12	102 ± 1.28	101 ± 0.699	98.1 ± 4.58	99.3 ± 2.39
7 days	96.4 ± 4.28	104 ± 2.52	97.6 ± 3.45	98.2 ± 0.842	100 ± 6.59	101 ± 0.287	105 ± 1.12	104 ± 1.24
14 days	90.1 ± 1.78	92.8 ± 2.19	79.1 ± 1.50	81.0 ± 2.99	92.0 ± 2.10	91.8 ± 3.92	96.3 ± 4.20	94.9 ± 2.26
28 days	94.8 ± 2.09	92.1 ± 1.99	74.0 ± 0.764	76.4 ± 2.76	94.8 ± 3.14	95.6 ± 2.18	98.4 ± 1.59	101 ± 3.45
56 days	95.6 ± 3.10	94.1 ± 4.18	67.1 ± 2.84	68.5 ± 3.89	95.1 ± 4.15	94.8 ± 3.39	97.6 ± 3.48	97.7 ± 2.49

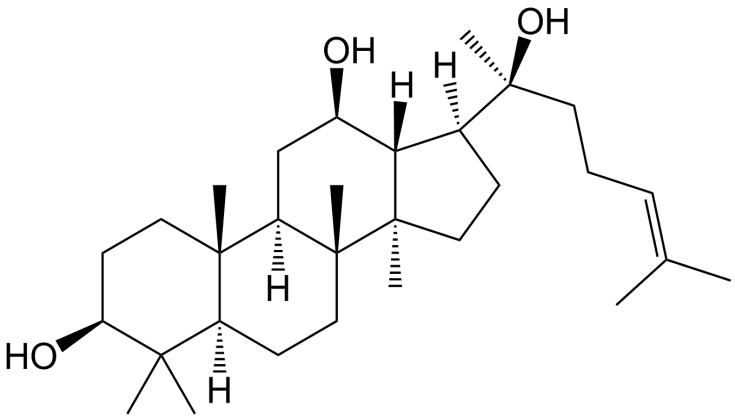

Figure 1 Chemical structure of 20(S)-protopanaxadiol (20S-PPD).

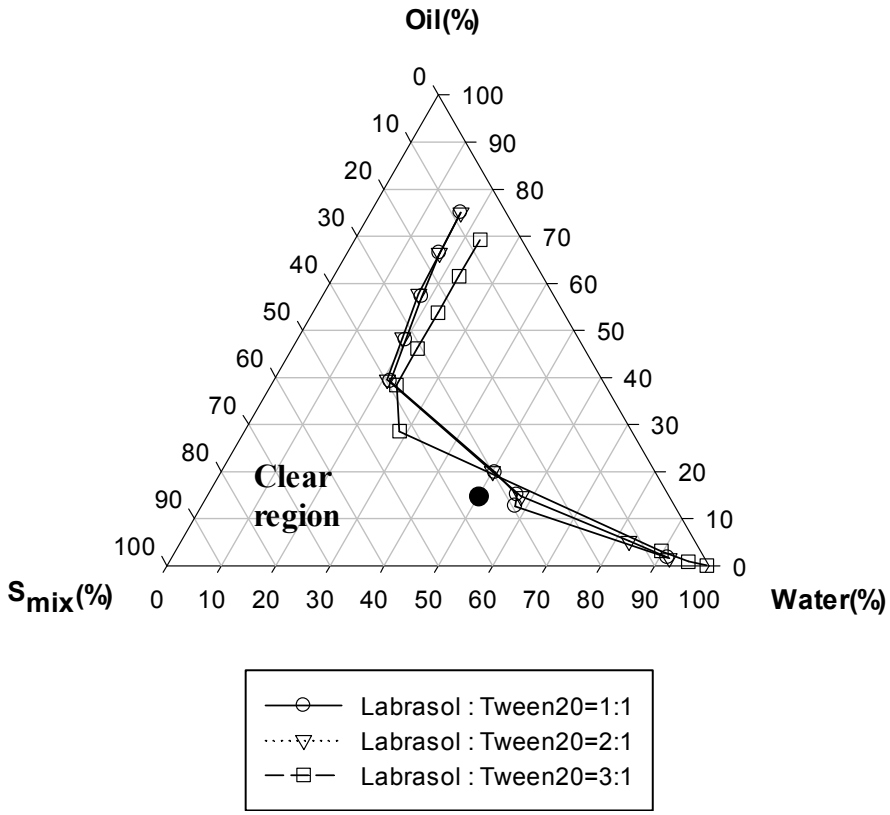

Figure 2 Pseudo-ternary phase diagrams of water, Capmul MCM EP (oil), and surfactant mixture (S_{mix}). The S_{mix} was the mixture of Labrasol and Tween 20 at 1:1, 2:1, and 3:1 ratio (w/w). Transparent MEs were formed in the clear region, and the other region represents turbid emulsions. The closed circle represents the compositions of ME formulations prepared with the three different S_{mix} ratios (1:1, 1:2, 1:3 for P1, P2, and P3, respectively).

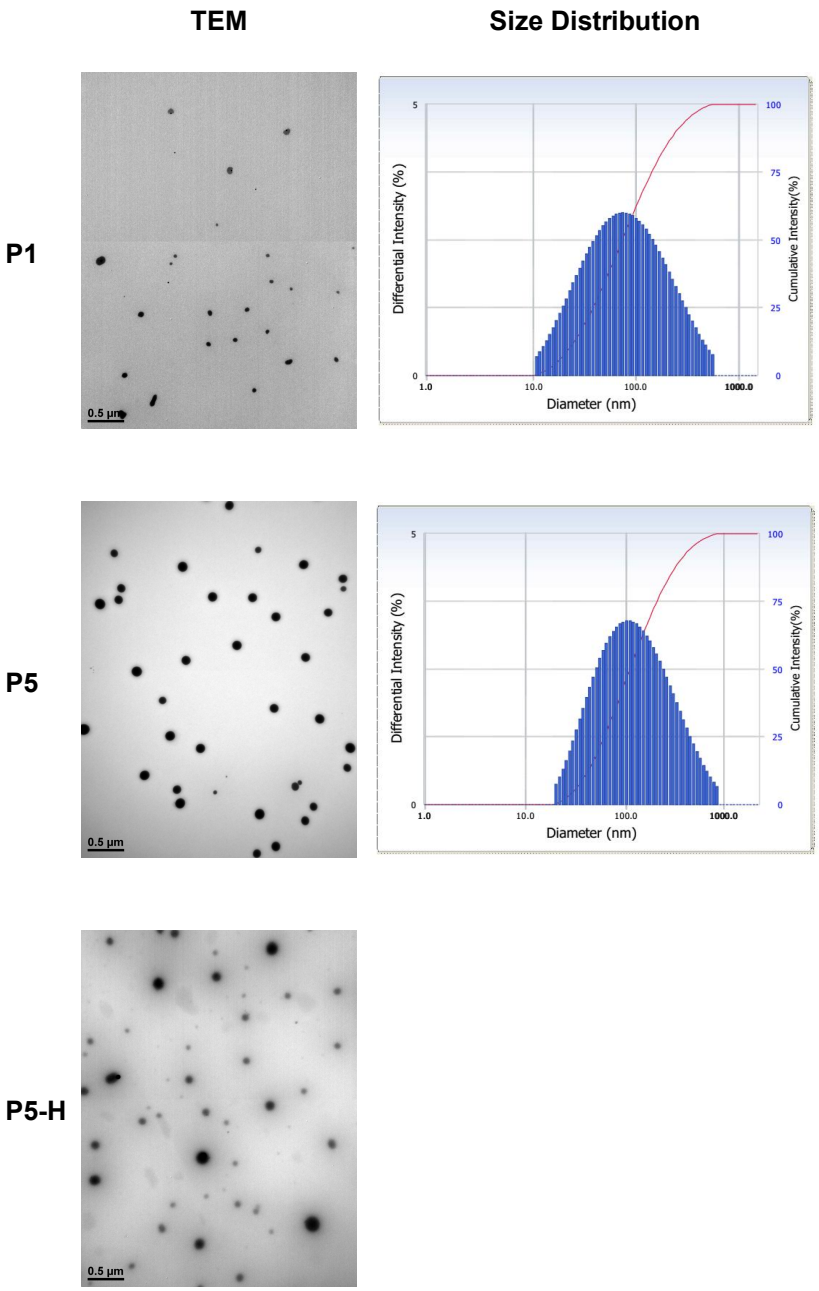

Figure 3 TEM images and particle size distribution of 20S-PPD-loaded ME and MEH formulations. The scale bars represent 0.5 µm.

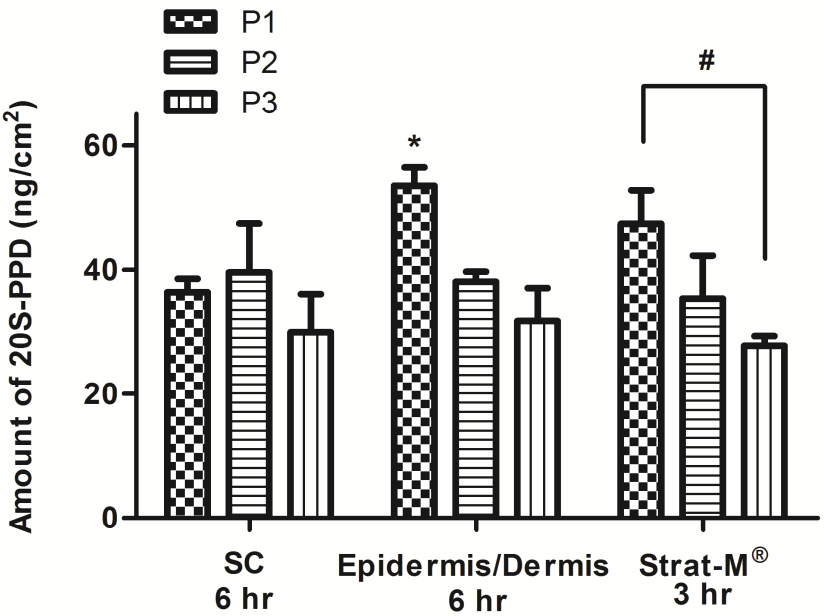

Figure 4 *In vitro* deposition of 20S-PPD in the stratum corneum (SC) and epidermis/dermis of hairless mouse skin at 6 hr and that in Strat-M® membrane at 3 hr after the topical administration of P1, P2, and P3 at the concentration of 0.1% (w/w). The rectangular bars and their error bars represent the means and standard deviations, respectively (n = 3). The asterisk represents a value significantly different from that of the other groups, and the pound sign represents a significant difference between the two groups indicated ($p < 0.05$).

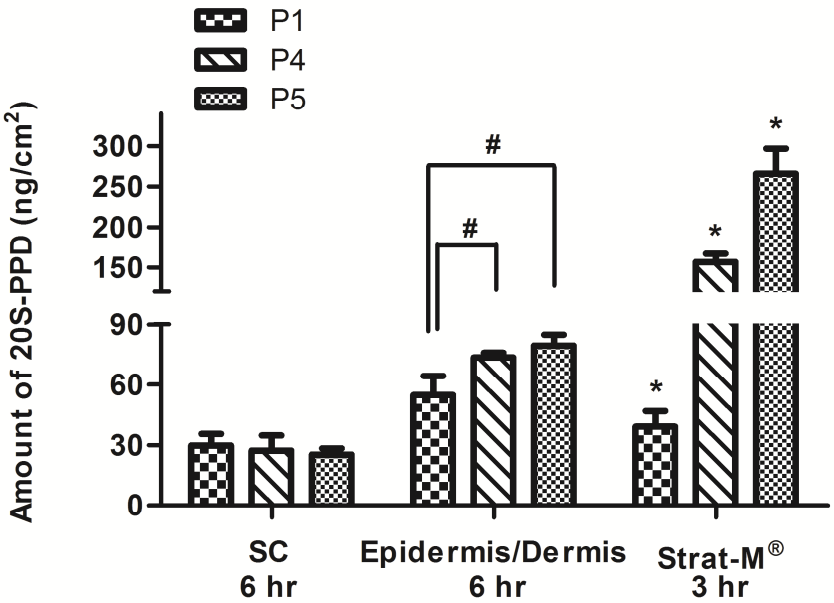

Figure 5 *In vitro* skin deposition of 20S-PPD in the stratum corneum (SC) and epidermis/dermis of hairless mouse skin at 6 hr and in Strat-M® membrane at 3 hr after the topical administration of P1, P4, and P5 at the concentration of 0.1% (w/w). The rectangular bars and their error bars represent the means and standard deviations, respectively (n = 3). The asterisk represents a value significantly different from that of the other groups, and the pound sign represents a significant difference between the two groups indicated ($p < 0.05$).

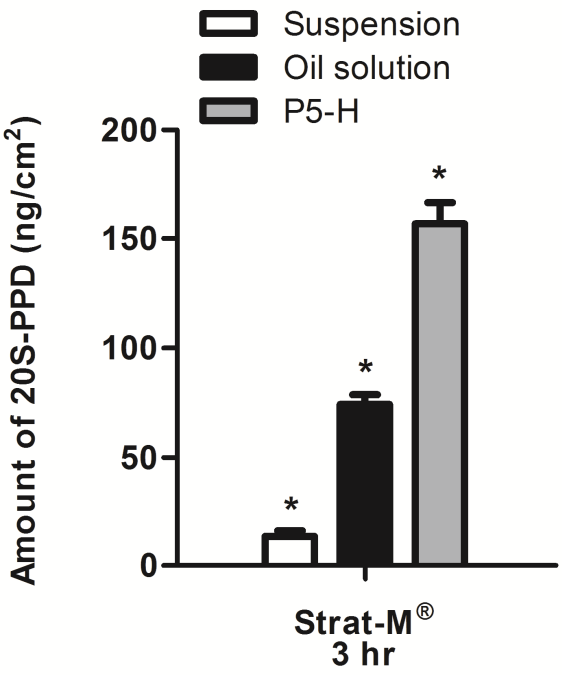

Figure 6 *In vitro* deposition of 20S-PPD in Strat-M® membrane at 3 hr after the topical administration of suspension, oil solution, and P5-H at the 20S-PPD concentration of 0.1% (w/w). The rectangular bars and their error bars represent the means and standard deviations, respectively (n = 3). The asterisk represents a value significantly different from that of the other groups (p < 0.05).

(A) Stratum corneum (SC)

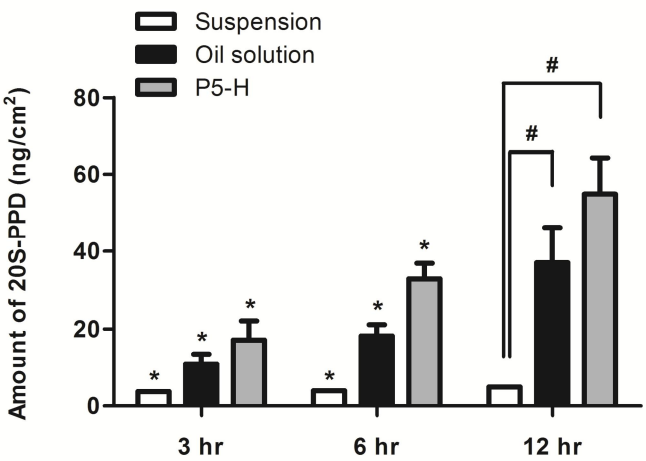

(B) Epidermis/Dermis

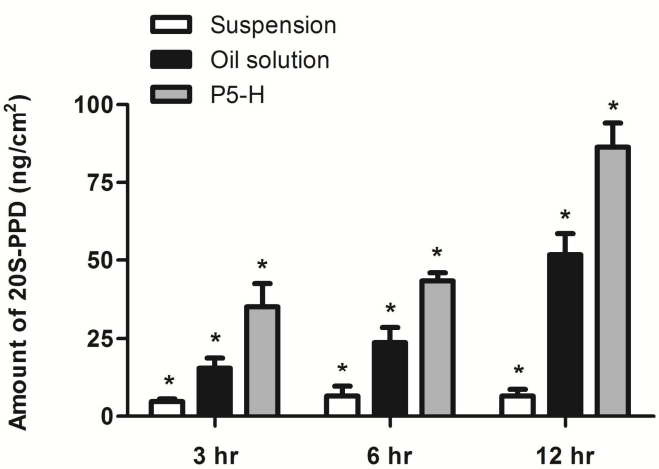

Figure 7 *In vivo* skin deposition of 20S-20S-PPD at 3, 6, and 12 hr in the stratum corneum (A) and epidermis/dermis (B) of hairless mouse skin after the topical administration of suspension, oil solution, and P5-H containing 0.1% (w/w) 20S-PPD at a dose of 25 mg/kg. The rectangular bars and their error bars represent the means and standard deviations, respectively (n = 3). The asterisk represents a value significantly different from that of the other groups, and the pound sign represents a significant difference between the two groups indicated ($p < 0.05$).

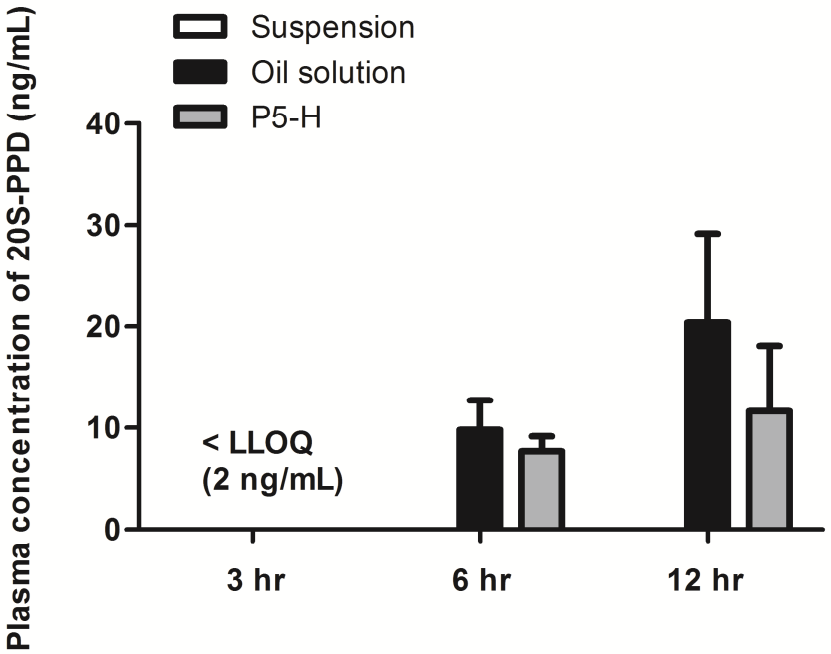

Figure 8 *In vivo* plasma concentration levels of 20S-PPD at 3, 6, and 12 hr after the topical administration of suspension, oil solution, and P5-H containing 0.1% (w/w) 20S-PPD at a dose of 25 mg/kg in hairless mice. The rectangular bars and their error bars represent the means and standard deviations, respectively (n = 3).

(A)

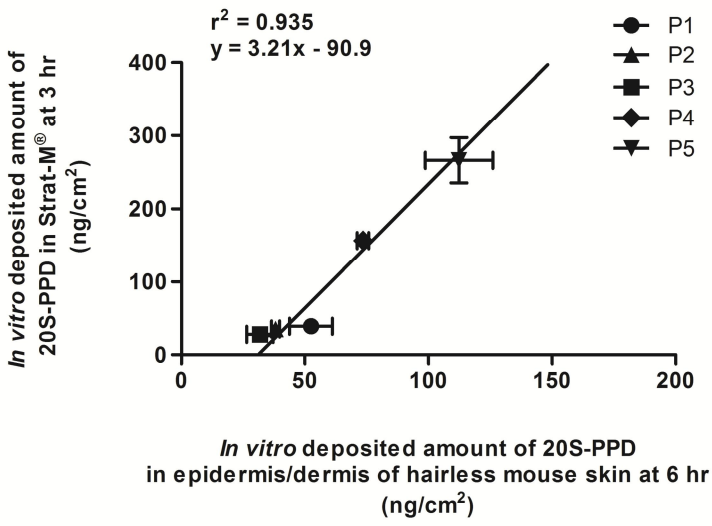
r² = 0.935
y = 3.21x - 90.9
P1
P2
P3
P4
P5
In vitro deposited amount of 20S-PPD in Strat-M® at 3 hr (ng/cm²)
400
300
200
100
0
0
50
100
150
200
In vitro deposited amount of 20S-PPD in epidermis/dermis of hairless mouse skin at 6 hr (ng/cm²)

(B)

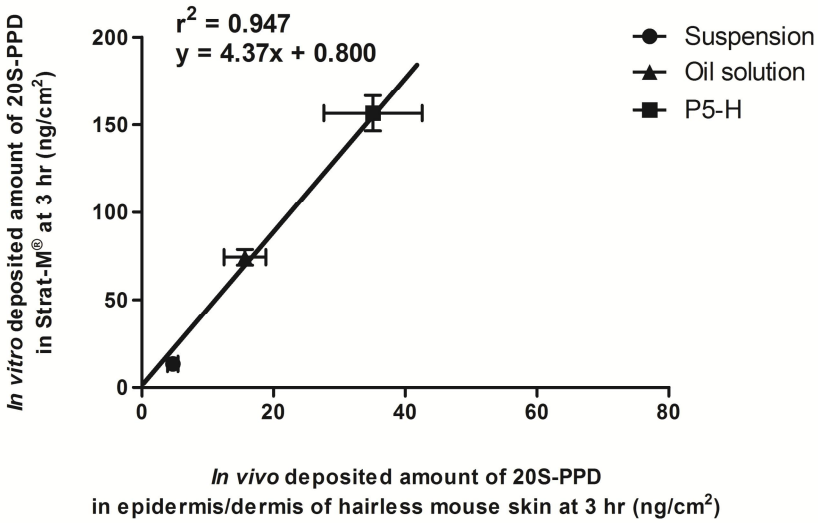
r² = 0.947
y = 4.37x + 0.800
Suspension
Oil solution
P5-H
In vitro deposited amount of 20S-PPD in Strat-M® at 3 hr (ng/cm²)
200
150
100
50
0
0
20
40
60
80
In vivo deposited amount of 20S-PPD in epidermis/dermis of hairless mouse skin at 3 hr (ng/cm²)

(C)

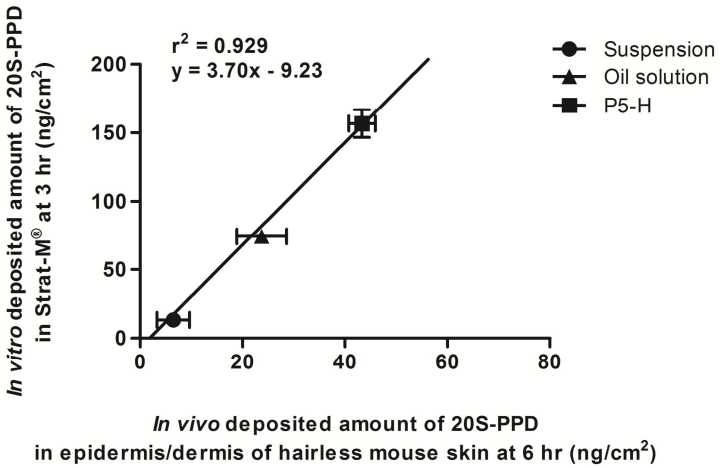

(D)

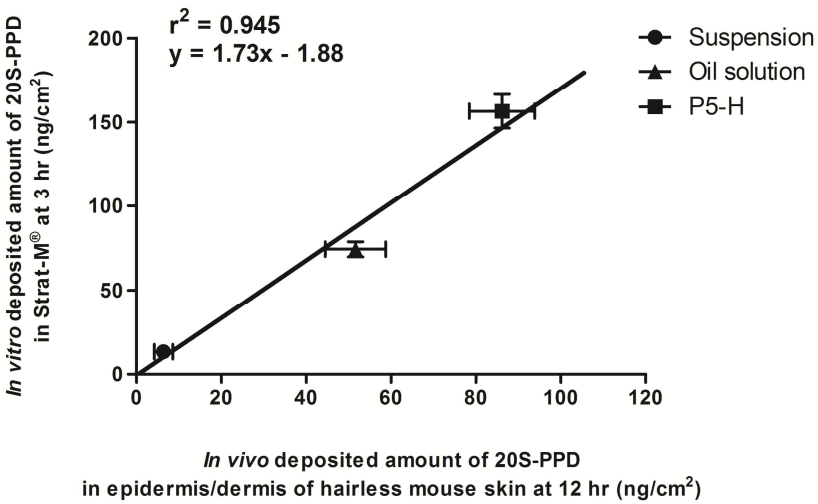

Figure 9 Correlation of the *in vitro* deposited 20S-PPD amounts at 3 hr in Strat-M® membrane with the *in vitro* deposited 20S-PPD amounts at 6 hr (A) and *in vivo* deposited 20S-PPD amounts at 3 hr (B), 6 hr (C), and 12 hr (D) in the epidermis/dermis of hairless mouse skin. The bullet symbols and their error bars represent the means and standard deviations, respectively (n = 3). The solid lines represent the fitted linear regression curves. The solid lines represent the fitted linear regression curves.

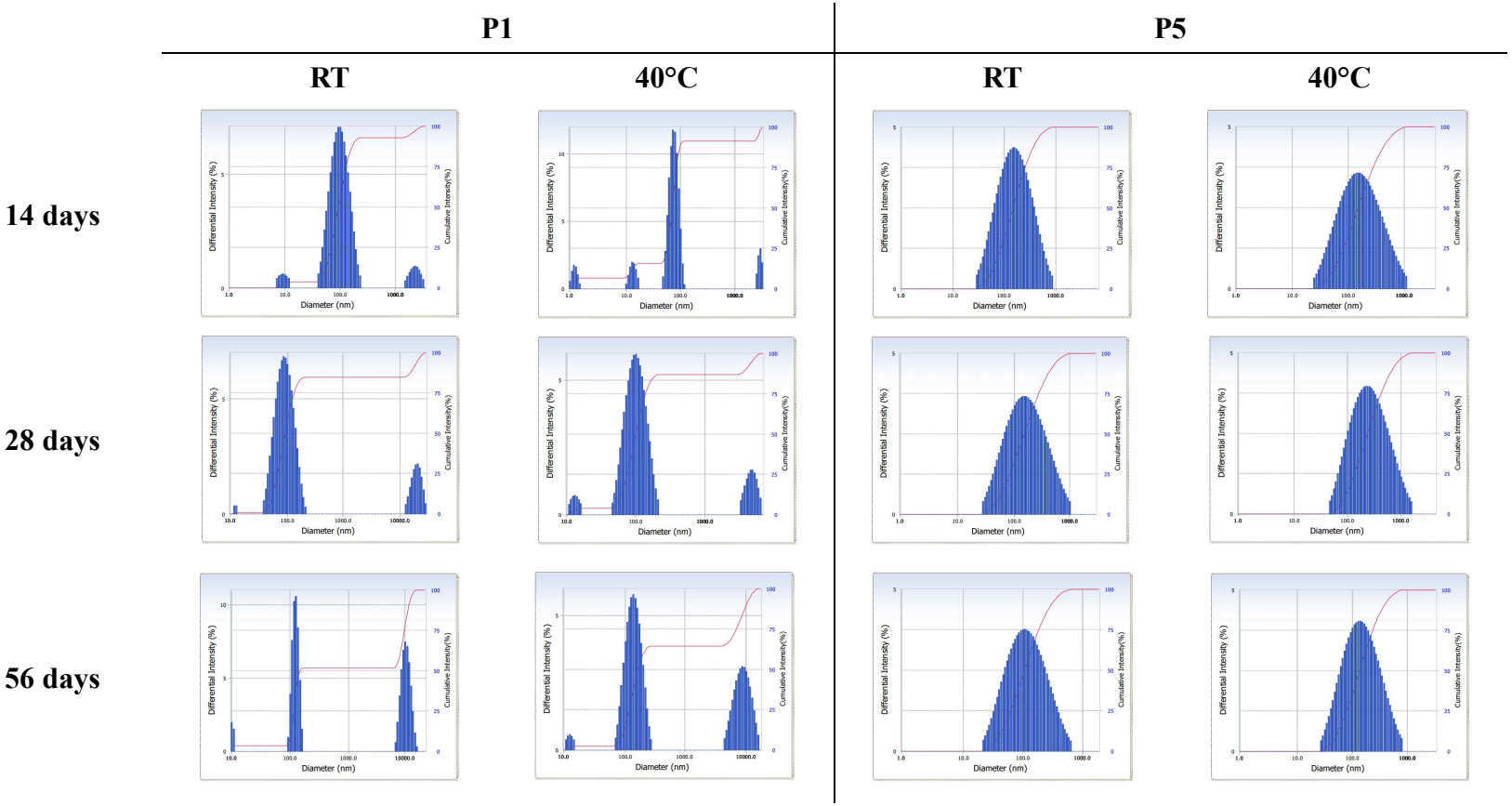

Figure 10 Particle size distribution of P1 and P5 stored at room temperature (RT) and 40°C for 14, 28, and 56 days.

Part II. Capmul MCM EP/Solutol HS 15-based microemulsion for enhanced oral bioavailability of rebamipide

1. Introduction

Water solubility of drug is an important factor for the absorption into the gastro-intestinal (GI) tract after oral administration [59]. Although there are complicate mechanisms on the oral absorption into GI tract including active transporter (*i.e.* organic cation transporters and organic anion polypeptide transporters) and efflux pump (*i.e.* p-glycoprotein), the passive diffusion through the membrane of GI tract is known to be the main absorption mechanism [60]. Therefore, poorly water-soluble agents, which can be included in the biopharmaceutics classification system (BCS) class II (low solubility, high permeability) and IV (low solubility, low permeability), could have low bioavailability because of their low absorption into GI tract [61,62]. Also, low solubility can cause large fluctuations on the absorbed into GI tract followed by large variation between individuals [63]. Based on the Fick's laws, low absorption into the GI tract by the low aqueous solubility could affect the reduction of pharmacological efficacy at an administrated dose [5]. Therefore, solubilization techniques are essential for enhancing oral absorption of poorly water-soluble compounds and developing clinically- or commercially-useful delivery systems.

Rebamipide (RBP, Fig. 1) has diverse pharmacological activities on the stomach such as anti-ulcer, anti-oxidative, and anti-inflammatory effects [64-66]. RBP was reported to have anti-ulcer activity by increasing prostaglandin levels as increasing the gene expression of cyclooxygenase-2 and decreasing that of prostaglandin dehydrogenase in gastric epithelial cells [64]. Previous studies were also demonstrated that RBP had anti-oxidative effect by reducing oxygen-derived

free radical produced by neutrophils in gastric epithelial cells and blood vessels [65]. Besides, RBP inhibited several inflammation mechanisms in the blood capillary by prohibiting adhesion of neutrophil to endothelial cells and its migration into the tissue [66]. Thus, following the oral dosing of RBP, its systemic absorption into the blood circulation or local penetration into the gastric epithelial cells is an essential prerequisite for exerting its pharmacological activities.

However, RBP was classified as a BCS class IV drug which presented a low solubility and permeability [67]. Due to its limited aqueous solubility and permeability, RBP has a low oral bioavailability of less than 10%, which may cause difficulties in optimizing RBP-based therapy [67]. In order to overcome this limitation, solid dispersions and nanocrystal formulations were prepared to enhance the solubility/dissolution and oral bioavailability of RBP in previous studies [68,69]. However, there still exists the necessity of further attempts to develop more efficient oral RBP formulations.

Amongst various drug delivery systems, ME systems has higher drug loading capacity by solubilizing water-insoluble drug in the oil phase and can present the enhancement of drug permeation into GI tract by the action of S_{mix} phase [8,11]. For these reasons, ME systems have been reported to significantly enhance the solubility/dissolution and oral bioavailability of several BCS class IV drugs including docetaxel and cefpodoxime [26,70]. However, to the best of our knowledge, there have been few studies on the development of ME systems for the enhanced oral absorption of RBP. Therefore, ME systems were studied as drug delivery systems for the enhanced oral delivery of RBP in the present study.

Herein, we report on the development of ME formulations to enhance

oral delivery of RBP. The RBP-loaded ME formulations were prepared by the construction of pseudo ternary phase diagram and characterized *in vitro* in terms of loading capacity, particle-size distribution, morphology, surface charge. The *in vitro* drug release study and *in vivo* pharmacokinetic study were performed to present the enhancement of dissolution and oral bioavailability of RBP compared to its suspension. Finally, the *in vivo* toxicity of RBP-loaded ME after the oral administration was also studied.

2. Materials and Methods

2.1. Materials

Rebamipide (RBP) was supplied by Hanlim Pharm. Co., Ltd. (Seoul, Korea). Capmul MCM EP was gifted as a sample from ABITEC Co. (Columbus, OH, USA). Lauroglycol CC, Transcutol HP, Capryol 90, and Labrafil WL 2609 BS were gifted as samples from Gattefossé Co. (Saint Priest, Cedex, France). Solutol HS 15, sodium lauryl sulfate (SLS), and naproxen were purchased from Sigma-Aldrich Chemical Co. (St. Louis, MO, USA). Tween 80 was purchased from Tokyo Chemical Industry Co., Ltd. (Tokyo, Japan). HPLC grade methanol and acetonitrile were purchased from Thermo Fisher Scientific Co. (Pittsburgh, PA, USA). All other reagents were of analytical grade.

2.2. Animal

Male Sprague-Dawley (SD) rats (200-250 g) (Orient Bio, Inc., Seongnam, Korea) were used to evaluate *in vivo* pharmacokinetic profile and intestinal toxicity of RBP formulatons. They were bred on sawdust and five mice were in each cage. They had free access to water and food before the studies. Room illumination was on an automatic cycle of 12 hr light/darkness, and room temperature was maintained at 25 ± 2°C. They were acclimatized to the presented conditions for at least one week prior to the experiments. Experimental protocols for the animals

(Approval number: SNU-160311-3-1) used in this study were reviewed by the Animal Care and Use Committee of the College of Pharmacy, Seoul National University and were in accordance with the National Institutes of Health's Guide for the Care and Use of Laboratory Animals (National Institutes of Health Publication Number 85-23, revised 1985).

2.3. Solubility study

The equilibrium solubility of RBP in various vehicles was determined by adding excess amount of them into 1 mL of each vehicle. The mixtures containing RBP were placed in a shaking incubator (BS-21; Jeio Tech. Co. Ltd., Seoul, Korea) with 50 rpm at 37°C for 72 hr. The samples were centrifuged at 16,000 x *g* for 5 min and the supernatant was filtrated with 0.20 μm syringe filter to remove the excess amount of RBP. Finally, the concentration of RBP in the filtrated solution was quantified by HPLC-fluorescence after appropriate dilution with methanol.

2.4. Construction of pseudo-ternary phase diagrams

Based on the solubility test of RBP (Table 1), Capmul MCM EP was selected as an oil phase, Solutol HS 15 or Tween 80 were selected as a surfactant, and Transcutol or ethanol were selected as a co-surfactant. The pseudo-ternary phase diagram studies were performed to find a clear and transparent ME formulations. The surfactant and co-surfactant were mixed at different ratios to

form the surfactant mixture (S_{mix}). Afterwards, the oil phase and the S_{mix} were mixed, where the ratios of oil to S_{mix} were varied as 9:1, 8:2, 7:3, 6:4, 5:5, 4:6, 3:7, 2:8, and 1:9 (w/w). Then, the water phase (distilled water, DW) was added drop-wise to each oil and S_{mix} mixture at room temperature with stirring to allow equilibration. After equilibrium, the mixtures were visually checked for transparency. The points from clear to turbid state were presented on the diagrams.

2.5. Preparation of RBP-loaded MEs

From the clear region of pseudo-ternary phase diagrams, four ME formulations (R1–R4) were selected for further evaluations (Table 2). For the preparation of MEs of 0.1% (w/w) RBP, exact amount of RBP was first added into Capmul MCM EP and vortex-mixed to dissolve RBP. Then, S_{mix} which was the different combination of surfactant and co-surfactant (Solutol HS 15 and ethanol, Solutol HS 15 and transcutol, Tween 80 and ethanol, or Tween 80 and transcutol) was subsequently added to the oil solution containing RBP under gentle stirring at 37°C. Afterwards, DW was added dropwise into the above mixture at the same condition.

2.6. Characterization of RBP-loaded MEs

2.6.1. Maximum loading capacity

To confirm the maximum RBP-loading capacity of ME formulations, excess RBP was added into the mixture of oil and S_{mix}, after which the RBP-loaded MEs were prepared as the same method before. Then, excess RBP which was not included into the droplets of ME was removed by centrifugation for 5.0 min at 16,000 x *g*. The supernatant was injected into HPLC-fluorescence for analysis of RBP after adequate dilution with methanol.

2.6.2. Particle size and zeta potential

The mean particle size, polydispersity index, intensity distribution of particle size, and zeta potential of blank ME and RBP-loaded ME (R1) were measured in triplicate by ELS spectrophotometer (ELS 8000, Otsuka Electronics Co. Ltd., Tokyo, Japan). The prepared MEs were transferred to a quartz cuvette before the measurement. All measurements were performed at 25°C in triplicate. Besides, in order to estimate the changes in RBP-loaded ME after the oral administration, mean droplet size of diluted R1 formulation with pH 1.2 buffer to 10 and 100-fold was also measured by ELS spectrophotometer.

2.6.3. TEM

The particle morphologies of blank ME and R1 were observed by an energy-filtering transmission electron microscopy (TEM) (LIBRA 120, Carl Zeiss, Germany) at 80 kV. The samples were placed on a carbon-coated copper grid and

negatively stained by 2% phosphotungstic acid followed by drying at room temperature before the operations.

2.7. In vitro drug release study

The *in vitro* drug release study of RBP-loaded ME (R1) in various pH buffers compared to its suspension was performed by dialysis method [26]. An aliquot (200 μL) of each ME formulation (R1) and suspension in DW containing 0.1% (w/w) RBP was placed in the dialysis kits (GeBA tubes, molecular weight cut-off: 14 KDa; Gene Bio-Application Ltd., Kfar-Hanagid, Israel). Then, the kits was immersed in 20 mL of release media (pH 1.2, 4.0, and 6.8 buffer solution containing 0.2% SLS (w/v) to maintain sink condition) in a shaking incubator (BS-21) at 100 rpm at 37°C. At pre-determined time points, a 200-μL aliquot of media was collected and replaced with same volume of fresh media. The concentration of RBP in samples was determined by using HPLC-fluorescence after appropriate dilution with methanol.

2.8. In vivo pharmacokinetic study

Before the experiment, the rats were fasted overnight with access to water. The femoral artery of the rats was cannulated with a polyethylene tube (Becton Dickinson Diagnostics, Sparks, MD, USA) under anesthesia with Zoletil (20 mg/kg, intramuscular injection) (Virbac, Carros, France) [71]. ME formulation (R1) and

suspension in DW containing 0.1% (w/w) RBP were directly administered to the stomach of rats using an oral sonde at a dose of 5 mg/kg. An approximately 250 μL aliquot of blood samples was withdrawn from the femoral artery at pre-determined time points (5, 15, 30, 45, 60, 75, 90, 120, 180, 240, and 360 min). The same volume of heparinized normal saline (20 IU/mL) was used to flush the cannula immediately after each blood sampling to prevent a blood clotting. Plasma samples were obtained by centrifugation of the blood samples at 16000 ×*g* for 5 min and stored at –20°C until HPLC analysis.

2.9. In vivo intestinal toxicity study

In order to evaluate the intestinal toxicity of RBP formulations, the jejunum (approximately 5 cm) of rats was carved out at 24 hr after the oral administration of DW, blank ME, RBP suspension, and RBP-loaded ME (R1). The segment was washed with PBS and fixed in 4% paraformaldehyde for 24 hr. A vertical section of jejunum was stained with hematoxylin-eosin (H&E) and observed using an optical microscope (×200).

2.10. HPLC-fluorescence analysis of RBP

Plasma samples containing RBP were allowed to thaw at room temperature for analysis. A 100-μL aliquot of plasma samples was deproteinized with a 200-μL aliquot of MeOH containing 10 μg/mL naproxen as an internal

standard. After vortex-mixing and centrifugation, a 20-μL aliquot of the supernatant was injected into HPLC system. The HPLC system consisted of a Waters 2475 Multi λ Fluorescence Detector, e2695 Separations Module, and Gemini C18 column (250×4.60 mm, 5 μm; Phenomenex, Torrance, CA, USA). The wavelength of the fluorescence detector was set at 320 nm as excitation and 380 nm as emission. The mobile phase, the mixture of ACN containing 0.1% TEA (v/v) and 10 mM KH_2PO_4 (77:23, v/v), was run at a flow rate of 1 mL/min. The calibration standard samples were prepared by spiking working standard into the blank plasma, thereby yielding final concentration range of 10.0–1000 ng/mL. The response of detector was linear in the concentration range and the mean correlation coefficient (r^2) for the calibration curve was over 0.999. The signal to noise ratio at the LLOQ (10.0 ng/mL) was higher than 5.0 and there was no interference from any other substances.

.

2.11. Statistical analysis and data analysis

All experiments in this study were performed at least three times, and the data are presented as mean ± standard deviation (SD). Statistical analyses were carried out using the two-tailed unpaired Student's *t*-test and $p < 0.05$ was considered significantly different. Non-compartmental analysis (WinNonlin, version 3.1, Pharsight Co., Mountainveiw, CA, USA) was performed to calculate the following pharmacokinetic parameter: the total area under the plasma concentration *versus* time curve from time zero to last time (360 min) (AUC_{last}). The peak plasma concentration (C_{max}) and time to reach C_{max} (T_{max}) were read

directly from the experimental data [71].

3. Results

3.1. Preparation of RBP- loaded MEs

RBP presented a low aqueous solubility in DW (0.01 mg/mL, Table 1). Below pH 5.0, its solubility was under 0.037 mg/mL, whereas at pH 7.0 to 8.0, that was significantly increased to 2.9 – 4.3 mg/mL (Fig. 2). Due to a low aqueous solubility of RBP in DW and acidic pH buffer, various oils and surfactants were tested to select suitable vehicles for RBP. The rank of the tested compounds in the order of decreasing solubility of RBP was as follows: Capmul MCM EP > Capryol 90 > Labrafil WL 2609 BS > Lauroglycol FCC as oils; Solutol HS 15 > Tween 80 > transcutol > ethanol as surfactants (Table 1). The pseudo-ternary phase diagrams consisting of water (DW), oil (Capmul MCM EP), and S_{mix} are shown in Fig. 3. The S_{mix} was the mixture of Solutol HS 15 as surfactant and ethanol or transcutol as co-surfactant at 3:1 ratio (w/w). Another S_{mix} was the mixture of Tween 80 as surfactant and ethanol or transcutol as co-surfactant at 5:3 ratio (w/w). As shown in Fig. 3, the formation of clear and transparent MEs was observed in constructing the pseudo-ternary phase diagrams with all different S_{mix} combinations. Four different ME formulations were selected within the clear and transparent area of MEs prepared with the different S_{mix} combinations, *i.e.* R1, R2, R3, and R4 (Table 2).

3.2. Characterization of RBP-loaded MEs

The compositions of RBP-loaded ME formulations are listed in Table 2. Among those MEs (R1 to R4), the maximum loading capacity was highest in R1 (1.13 mg/mL), followed by R3, R2 and R4. The mean droplet size, polydispersity index, and zeta potential of blank ME and RBP-loaded ME (R1) are presented in

Table 3. The mean droplet size of both MEs was 86.4 nm, which was not significantly different with each other. Moreover, these droplet size were not affected by 10 and 100-fold dilution with pH 1.2 buffer. Surface charge of droplets was observed to near neutral in both ME formulations. As shown in Fig. 4, spherical and nano-sized particles with a narrow size distribution were observed in both MEs.

3.3. In vitro release of RBP

The time profiles of *in vitro* release of RBP from suspension and RBP-loaded ME (R1) are shown in Fig. 5. The cumulative release of RBP from suspension increased as the pH increased. At pHs 1.2 and 4.0, the extent and rate of release of RBP were markedly higher in R1 than suspension (Fig. 5a and 5b). However, at pH 6.8, the release rate of RBP was faster in suspension than R1, and the cumulative release of RBP was approximately 100% from both groups (Fig. 5c).

3.4. In vivo plasma concentration profiles of RBP after oral administration at the dose of 5 mg/kg in rats

The time profiles of *in vivo* rat plasma concentrations of RBP after the oral administration of suspension and RBP-loaded ME (R1) at a dose of 5 mg/kg are shown in Fig. 6, and relevant pharmacokinetic parameters are listed in Table 4. The C_{max} and AUC of RBP were significantly higher in R1 than suspension. The C_{max} of RBP was enhanced 5.7-fold in R1 as compared with that in suspension

(156 ng/mL *versus* 27.3 ng/mL; $p < 0.05$). The AUC of RBP in R1 also increased 4.2-fold compared with that in suspension (31.1 μg·min/mL *versus* 7.47 μg·min/mL; $p < 0.05$). However, the T_{max} of RBP was not significantly different between both groups.

3.5. In vivo intestinal toxicity after oral administration at the dose of 5 mg/kg in rats

The representative histological sections of jejunum segments at 24 hr after oral administration of DW (a), blank ME (b), RBP suspension (c), RBP-loaded ME (R1, d) to rat were presented on Fig. 7. In all group, any evidence of damage to the intestinal jejunum such as fusion of villus and congestion of mucosal capillary with blood was not found. Also, there was no distinguishable difference among all groups tested.

4. Discussion

The present study provided novel data on the development of ME formulation for the oral delivery of RBP in order to enhance its oral absorption. To prepare RBP-loaded ME formulations, Capmul MCM EP was selected as an oil phase due to its higher ability to solubilize RBP as compared to the other oils tested

(Table 1). Solutol HS 15 and Tween 80 were selected as the surfactant, due to their higher ability to solubilize RBP (Table 1). The S_{mix} was the mixture of high HLB surfactant (Solutol HS 15, HLB = 16.3; Tween 80, HLB = 15.0) and low HLB co-surfactant (Transcutol, HLB = 4.2) or ethanol in order to render ME systems to be more stable [8,45]. Moreover, ethanol can reduce the interfacial tension and improve the flexibility and stability of ME [72]. Based on the rule of high water portion and low oil/S_{mix} portion, as mentioned above, the RBP-loaded MEs (R1 to R4) were selected within the transparent ME area. Among those MEs, the maximum loading capacity was highest in R1 (1.13 mg/mL), which was markedly higher in comparison with the aqueous solubility of RBP in DW and acidic pH buffer (0.01 mg/mL in DW and 0.04 mg/mL in pH 5.0 buffer; Table 1 and Fig. 2). Thus, R1 was selected for further studies, and the loading content of RBP in R1 was set as 0.1% (w/w) in order to prevent aggregation and precipitation in ME system.

The physicochemical properties of the ME formulations containing RBP were characterized as presented in Table 3. The mean droplet size of RBP-loaded ME (R1) was not significantly different with that of blank ME (86.4 nm; Table 3), probably because RBP was fully-incorporated with in the droplets of ME, not dispersed in the water phase. Moreover, the change of mean droplet sizes of R1 after 10 and 100-fold dilution with pH 1.2 buffer was not significant (75.3 and 85.1 nm, respectively). Thus, it was expected that the prepared R1 would be stable in the gastric fluid after the oral administration. Also, the surface charges of droplets in blank ME and R1 prepared were near neutral (Table 3), probably because they consisted of non-ionic surfactants and oil. This may reduce the risk of irritations on

the GI tract, as mentioned above [52].

In vitro drug release profiles of RBP formulations were evaluated using the dialysis method (Fig. 5). Compared with RBP suspension, higher and faster release of RBP was observed in RBP-loaded ME (R1) at pH 1.2 and 4.0. It might be probably due to the solubility enhancing effect of the ME tested. However, at pH 6.8, where RBP can be freely soluble (3.3 mg/mL at pH 7.0; Fig. 2), the rate of RBP release was faster in suspension than in R1, while its extent was similar with both groups to almost 100%. This result may be attributed to the slow diffusion of RBP from the oil phase of ME formulation and the slow penetration process of RBP through the dialysis membrane due to the relatively high viscosity of R1 compared to suspension [43].

The *in vivo* oral pharmacokinetics of RBP formulations was evaluated using the rat model (Fig. 6), based on a good correlation regarding the absorption after oral administration between in rats and in humans [73]. In the *in vivo* rat pharmacokinetic study, the dose of RBP was set as 5 mg/kg. Oral administration of RBP at a dose of 5-10 mg/kg was used in several previous studies for the oral delivery of RBP [67-69]. After the oral administration of RBP formulations, systemic RBP exposures were significantly higher in RBP-loaded ME (R1) compared to suspension group, which is consistent with the *in vitro* drug release study. This improvement of RBP absorption may be attributed to the enhancement of its solubility and dissolution. Also, permeation-enhancing effects by the ingredients of ME could contribute to the improvement of RBP absorption [43]. It has been reported that Capmul MCM EP (medium chain mono- and di-glyceride) can acts as a membrane permeation enhancer [43,74]. Moreover, Solutol HS 15 has

been reported to enhance transepithelial permeability [75]. The intestinal toxicity of RBP formulations in rats was evaluated by histological H&E staining (Fig. 7). As shown in Fig. 7, no significant intestinal toxicity of RBP-loaded ME (R1) was observed compared with DW, RBP suspension, and blank ME. Thus, this result of *in vivo* intestinal toxicity study suggest that RBP-loaded ME formulation prepared in this study indicates a potentially safe oral delivery system for RBP.

5. Conclusion

In the present study, ME systems for enhancing the oral absorption of RBP were developed and evaluated via *in vitro* and *in vivo* studies. The ME formulation consisting of Capmul MCM, Solutol HS 15, and ethanol was prepared for the oral delivery of RBP based on the construction of pseudo-ternary phase diagram. The RBP-loaded ME had spherical nano-sized droplets with narrow size distribution and neutral zeta potential. Moreover, the prepared ME significantly

enhanced the dissolution and oral bioavailability of RBP with no discernible intestinal toxicity. Taken together, the ME systems developed in this study could serve as a potentially effective and safe oral delivery system for poorly soluble drugs including RBP.

Table 1 Solubility of RBP in various vehicles.

Type of phase	Vehicle	Solubility (mg/mL)
Water	Distilled water (DW)	0.01 ± 0.00
Oil	Capmul MCM EP	1.73 ± 0.39
	Capryol 90	0.17 ± 0.01
	Labrafil WL 2609 BS	0.10 ± 0.00
	Lauroglycol FCC	0.04 ± 0.00

Surfactant	Solutol HS 15	5.60 ± 0.04
	Tween 80	1.70 ± 0.02
	Transcutol	1.37 ± 0.40
	Ethanol	0.82 ± 0.01

Table 2 Weight compositions of ME formulations containing 0.1% (w/w) of RBP.

	Water	**Oil**	**Surfactant**	**Co-surfactant**
R1	DW (50)	Capmul (10)	Solutol (30)	Ethanol (10)
R2	DW (50)	Capmul (10)	Solutol (30)	Transcutol (10)
R3	DW	Capmul	Tween 80	Ethanol

	(45)	(15)	(25)	(15)
R4	DW (45)	Capmul (15)	Tween 80 (25)	Transcutol (15)

Table 3 Physicochemical properties of blank ME and RBP-loaded ME (R1).

Physicochemical property	Blank R1	R1
Particle size (nm)	86.4 ± 0.3	86.4 ± 1.8
Polydispersity index	0.274 ± 0.004	0.265 ± 0.006
Zeta potential (mV)	0.5 ± 0.1	0.8 ± 0.8

Table 4 Pharmacokinetic parameters of RBP after the oral administration of the RBP suspension and R1 at a dose of 5 mg/kg to rats (n=4).

Parameter	Suspension	R1
C_{max} (ng/mL)	27.3 ± 6.01	156 ± 40.6*
T_{max} (min)	15 (15–240)	30 (15–180)
AUC_{last} ($\times 10^3$ ng·min/mL)	7.5 ± 1.8	31.1 ± 13.6*

* Significantly different from the other groups ($p < 0.05$).

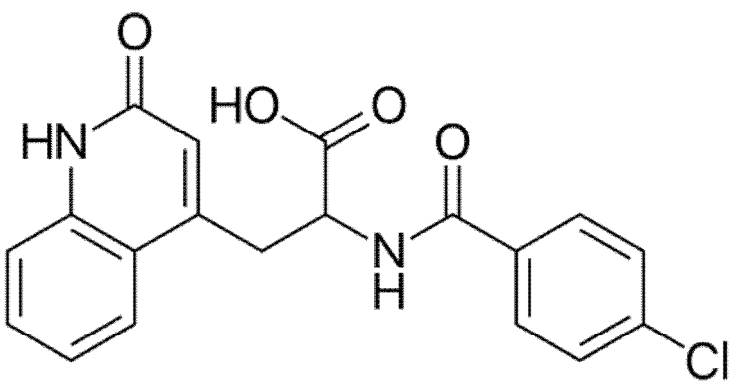

Figure 1 Chemical structure of rebamipide (RBP).

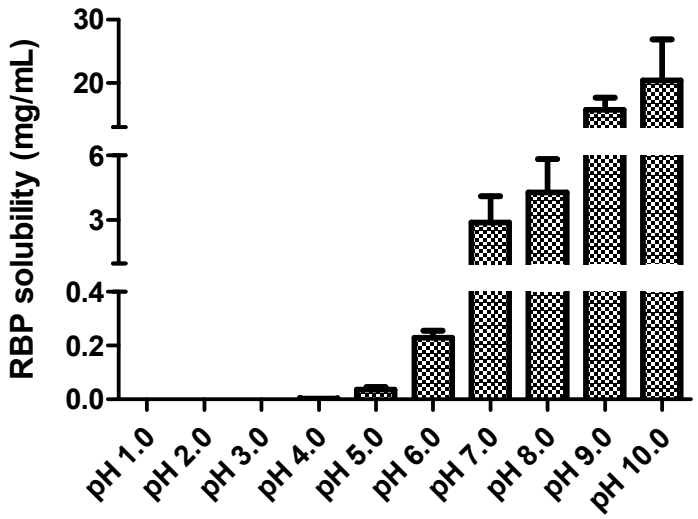

Figure 2 The solubility of RBP at various pH conditions.

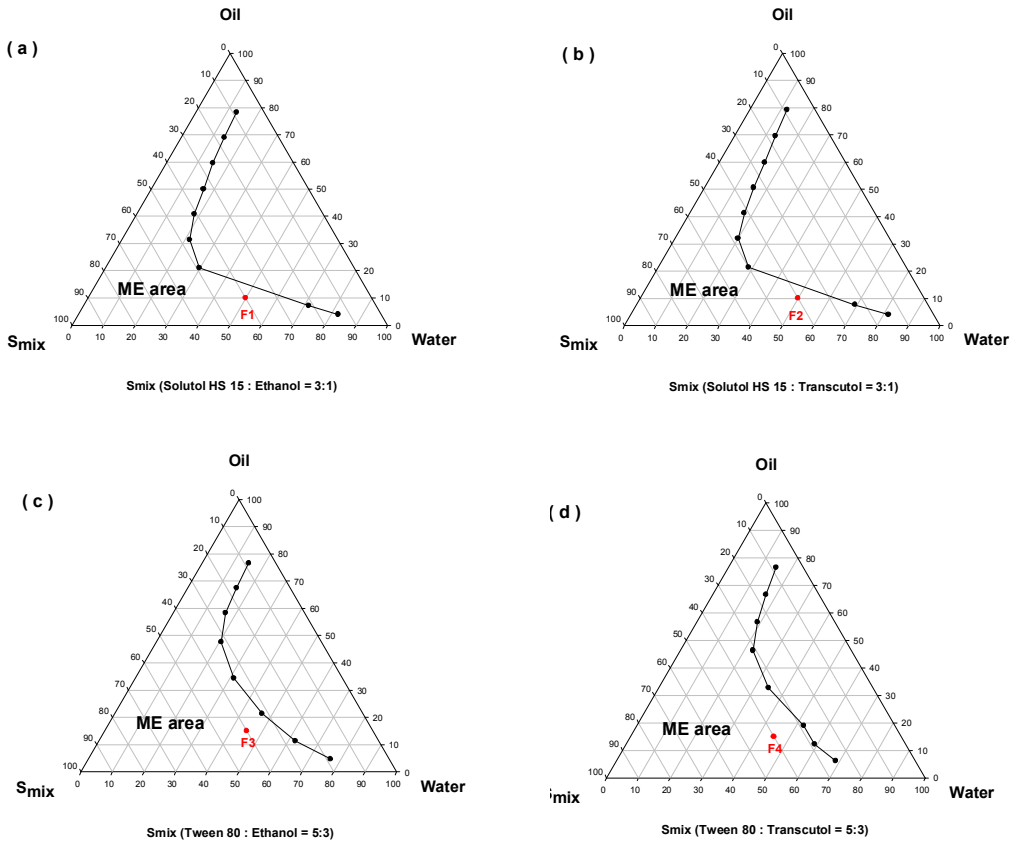

Figure 3 Pseudo-ternary phase diagrams of systems containing water, Capmul MCM EP (oil), and surfactant mixture (S_{mix}). The S_{mix} was the blend of Solutol HS 15 as surfactant and ethanol (a) or transcutol (b) as co-surfactant at 3:1 ratio (w/w). Another S_{mix} was the blend of Tween 80 as surfactant and ethanol (c) or transcutol (d) as co-surfactant at 5:3 ratio (w/w). Clear and transparent MEs were formed in the ME area, and other area represents turbid emulsion. The closed circles (●) represent the RBP MEs studied (R1, R2, R3, and R4).

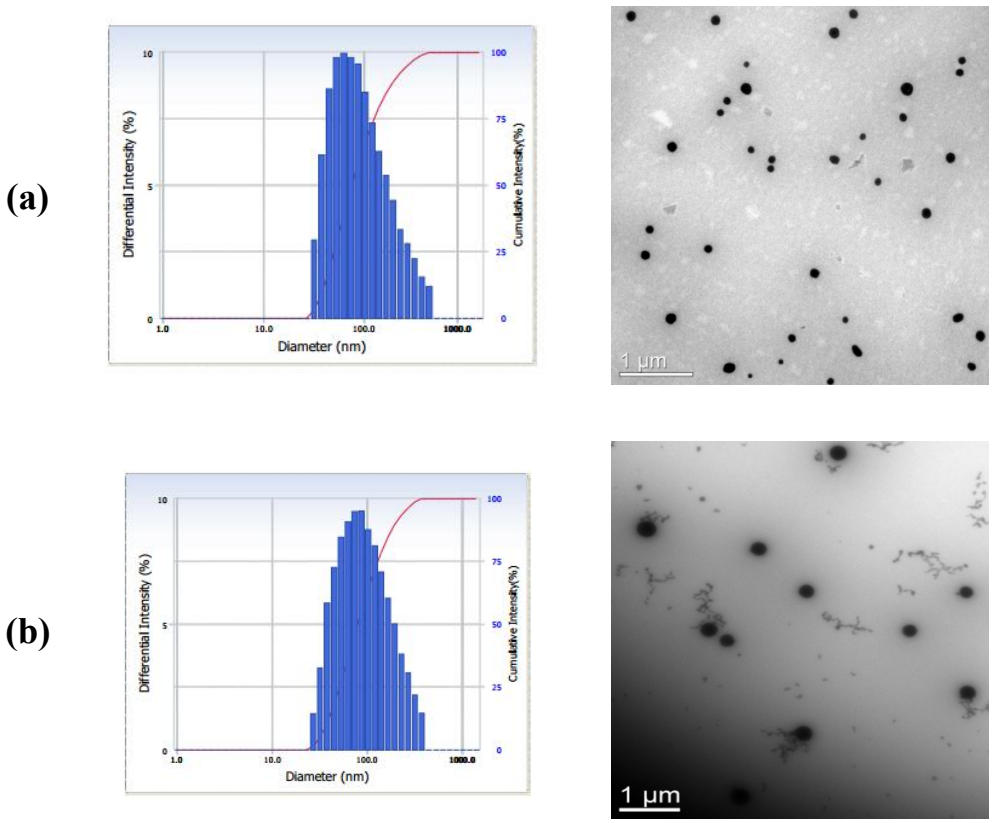

Figure 4 Intensity distribution diagrams of mean diameters and TEM images of RBP formulation (a, blank R1; b, RBP-loaded R1). The scale bars represent 1 µm.

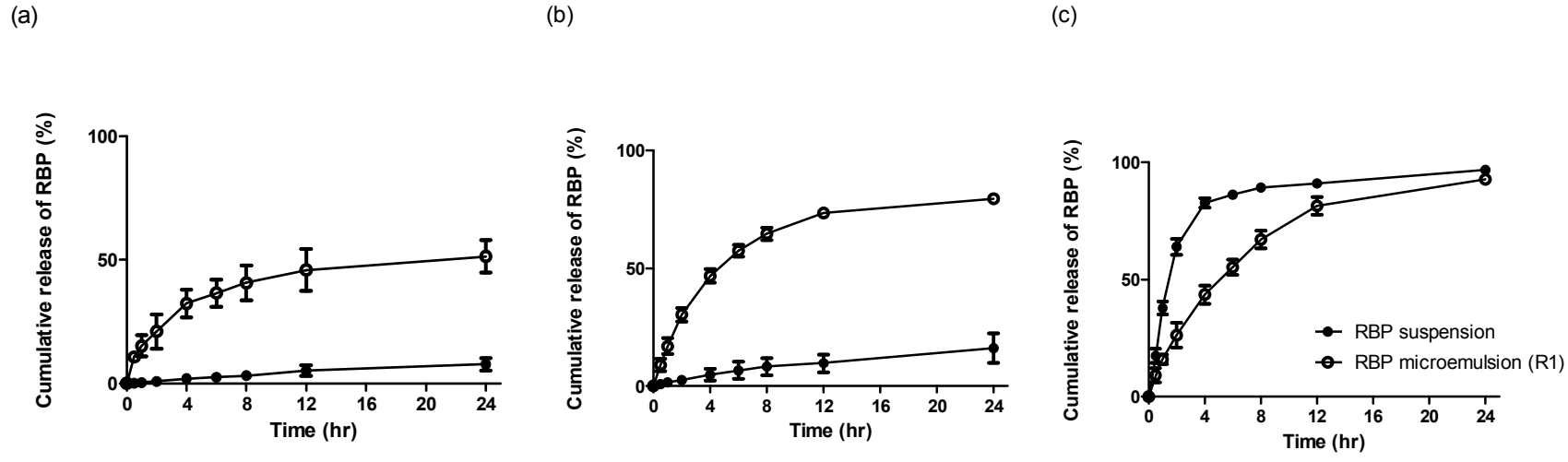

Figure 5 Time profiles of *in vitro* drug release of RBP from suspension (●), R1 (○) in pH 1.2 buffer (a), pH 4.0 buffer (b), and pH 6.8 buffer (c) containing 0.2% SLS (Mean ± SD).

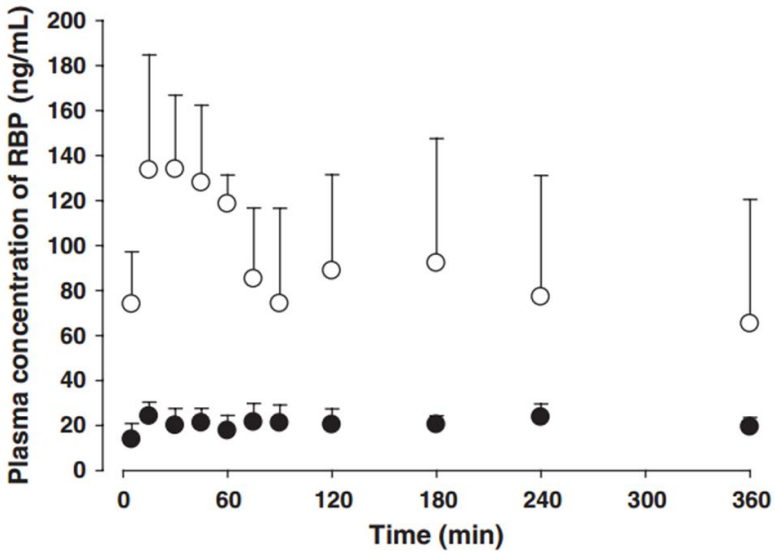

Figure 6 Time profiles of arterial plasma concentrations of RBP after oral administration of RBP suspension (●), R1 (○) at a dose of 5 mg/kg to rats (Mean ± SD, $n = 4$).

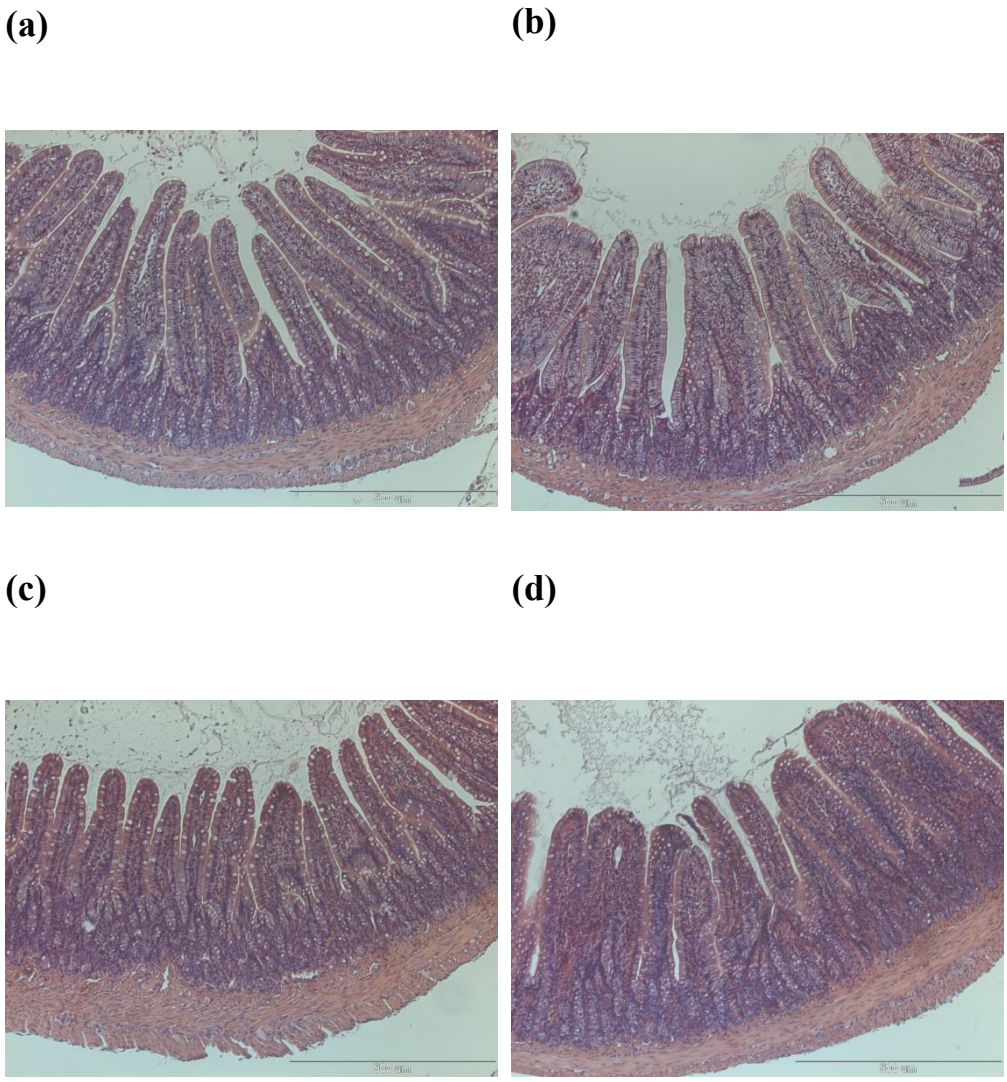

Figure 7 Representative histological sections of jejunal segments at 24 hr after oral administration of DW (a), blank R1 (b), RBP suspension (c), and R1 (d) to rats. The scale bars represent 500 μm.

References

[1] Scheuplein RJ. Mechanism of percutaneous adsorption: I. Routes of penetration and the influence of solubility. Journal of Investigative Dermatology. 1965;45:334-46.

[2] Scheuplein RJ. Mechanism of percutaneous adsorption: II. Transient diffusion and the relative importance of various routes of skin penetration. Journal of Investigative Dermatology. 1967;48:79-88.

[3] Marwah H, Garg T, Goyal AK, Rath G. Permeation enhancer strategies in transdermal drug delivery. Drug Delivery. 2016;23:564-78.

[4] Todo H, Oshizaka T, Kadhum WR, Sugibayashi K. Mathematical model to predict skin concentration after topical application of drugs. Pharmaceutics. 2013;5:634-51.

[5] Kalepu S, Nekkanti V. Insoluble drug delivery strategies: review on recent advances and business prospects. Acta Pharmaceutica Sinica B. 2015;5:442-53.

[6] Zhu W, Guo C, Yu A, Gao Y, Cao F, Zhai G. Microemulsion-based hydrogel formulation of penciclovir for topical delivery. Internatinal Journal of Pharmaceutics. 2009;378:152-8.

[7] Kansagra H, Mallick S. Microemulsion-based antifungal gel of luliconazole for dermatophyte infections: formulation, characterization and efficacy studies. Journal of Pharmaceutical Investigation. 2016;46:21-8.

[8] Lawrence MJ, Rees GD. Microemulsion-based media as novel drug delivery systems. Advanced Drug Delivery Reviews. 2012;64:175-93.

[9] Chen H, Chang X, Du D, Li J, Xu H, Yang X. Microemulsion-based hydrogel formulation of ibuprofen for topical delivery. International Journal of Pharmaceutics. 2006;315:52-8.

[10] Fanun M. Microemulsions as delivery systems. Current Opinion in Colloid & Interface Science. 2012;17:306-13.

[11] Hathout RM, Mansour S, Geneidi AS, Mortada ND. Visualization, dermatopharmacokinetic analysis and monitoring the conformational effects of a microemulsion formulation in the skin stratum corneum. Journal of Colloid and Interface Science. 2011;354:124-30.

[12] Constantinides PP, Lancaster CM, Marcello J, Chiossone DC, Orner D, Hidalgo I, Smith PL, Sarkahian AB, Yiv SH, Owen AJ. Enhanced intestinal absorption of an RGD peptide from water-in-oil microemulsions of different composition and particle size. Journal of Controlled Release. 1995;34:109-16.

[13] Vicentini FT, Simi TR, del Ciampo JO, Wolga NO, Iyomasa MM, Bentley MV, Fonseca MJ. Quercetin in w/o microemulsions: *in vitro* and *in vivo* skin penetration and efficacy against UVB-induced skin damages evaluated *in vivo*. European Journal of Pharmaceutics and Biopharmaceutics. 2008;69:948-57.

[14] Mei Z, Chen H, Weng T, Yang Y, Yang X. Solid lipid nanoparticle and microemulsion for topical delivery of triptolide. European Journal of Pharmaceutics and Biopharmaceutics. 2003;56:189-96.

[15] Jurkovic P, Sentjurc M, Gasperlin M, Kristl J, Pecar S. Skin protection against ultraviolet induced free radicals with ascorbyl palmitate in microemulsions. European Journal of Pharmaceutics and Biopharmaceutics. 2003;56:59-66.

[16] Raza K, Negi P, Takyar S, Shukla A, Amarji B, Katare OP. Novel dithranol

phospholipid microemulsion for topical application: development, characterization and percutaneous absorption studies. Journal of Microencapsulation. 2011;28:190-9.

[17] Cao FH, Ou-Yang WQ, Wang YP, Yue PF, Li SP. A combination of a microemulsion and a phospholipid complex for topical delivery of oxymatrine. Archives of Pharmacal Research. 2011;34:551-62.

[18] Jaiswal M, Kumar A, Sharma S. Nanoemulsions loaded Carbopol® 934 based gel for intranasal delivery of neuroprotective Centella asiatica extract: in–vitro and ex–vivo permeation study. Journal of Pharmaceutical Investigation. 2016;46:79-89.

[19] Lee SG, Kang JB, Kim SR, Kim CJ, Yeom DW, Yoon HY, Kwak SS, Choi YW. Enhanced topical delivery of tacrolimus by a carbomer hydrogel formulation with transcutol P. Drug Development and Industrial Pharmacy. 2016;42:1636-42.

[20] Dabhi MR, Nagori SA, Sheth NR, Patel NK, Dudhrejiya AV. Formulation optimization of topical gel formulation containing microemlsion of terbinafine hydrochloride with simplex lattice design. Micro and Nanosystems. 2011;3:1-7.

[21] El-Laithy HM, El-Shaboury KM. The development of Cutina lipogels and gel microemulsion for topical administration of fluconazole. AAPS PharmSciTech. 2002;3:77-85.

[22] Kantaria S, Rees GD, Lawrence MJ. Gelatin-stabilised microemulsion-based organogels: rheology and application in iontophoretic transdermal drug delivery. Journal of Controlled Release. 1999;60:355-65.

[23] Dreher F, Walde P, Luisi PL, Elsner P. Human skin irritation studies of a lecithin microemulsion gel and of lecithin liposomes. Skin Pharmacology. 1996;9:124-9.

[24] Jadhav KR, Shaikh IM, Ambade KW, Kadam VJ. Application of microemulsion based drug delivery system. Current Drug Delivery. 2006;3:267-73.

[25] Setthacheewakul S, Mahattanadul S, Phadoongsombut N, Pichayakorn W, Wiwattanapatapee R. Development and evaluation of self-microemulsifying liquid and pellet formulations of curcumin, and absorption studies in rats. European Journal of Pharmaceutics and Biopharmaceutics. 2010;76:475-85.

[26] Yin YM, Cui FD, Mu CF, Choi MK, Kim JS, Chung SJ, Skim CK, Kim DD. Doxetaxel microemulsion for enhanced oral bioavailability: preparation and *in vitro* and *in vivo* evaluation. Journal of Controlled Release. 2009;140:86-94.

[27] Nornoo AO, Zheng H, Lopes LB, Johnson-Restrepo B, Kannan K, Reed R. Oral microemulsions of paclitaxel: *in situ* and pharmacokinetic studies. European Journal of Pharmaceutics and Biopharmaceutics. 2009;71:310-7.

[28] Kang BK, Lee JS, Chon SK, Jeong SY, Yuk SH, Khang G, Lee HB, Cho SH. Development of self-microemulsifying drug delivery systems (SMEDDS) for oral bioavailability enhancement of simvastatin in beagle dogs. International Journal of Pharmaceutics. 2004;274:65-73.

[29] Kovarik JM, Mueller EA, van Bree JB, Tetzloff W, Kutz K. Reduced inter- and intraindividual variability in cyclosporine pharmacokinetics from a microemulsion formulation. Journal of Pharmaceutical Sciences. 1994;83:444-6.

[30] Kim K. Effect of ginseng and ginsenosides on melanogenesis and their mechanism of action. Journal of Ginseng Research. 2015;39:1-6.

[31] Han J, Lee E, Kim E, Yeom MH, Kwon O, Yoon TH, Lee TR, Kim K. Role of epidermal gammadelta T-cell-derived interleukin 13 in the skin-whitening effect of Ginsenoside F1. Experimental Dermatology. 2014;23:860-2.

[32] Wang L, Lu AP, Yu ZL, Wong RN, Bian ZX, Kwok HH, Yue PY, Zhou LM, Chen H, Xu M, Yang Z. The melanogenesis-inhibitory effect and the percutaneous formulation of ginsenoside Rb1. AAPS PharmSciTech. 2014;15:1252-62.

[33] Hong YH, Kim D, Hwang K, Yoo S, Han SY, Jeong S, Kim E, Jeong D, Yoon K, Kim S. Photoaging protective effects of BIOGF1K, a compound K-rich fraction prepared from Panax ginseng. Journal of Ginseng Research. 2017;in press(DOI: 10.1016/j.jgr.2017.01.002).

[34] Igami K, Ozawa M, Inoue S, Iohara D, Miyazaki T, Shinoda M, Anraku M, Hirayama F, Uekama K. The formation of an inclusion complex between a metabolite of ginsenoside, compound K and gamma-cyclodextrin and its dissolution characteristics. Journal of Pharmacy and Pharmacology. 2016;68:646-54.

[35] Kim EO, Cha KH, Lee EH, Kim SM, Choi SW, Pan CH, Um BH. Bioavailability of ginsenosides from white and red ginsengs in the simulated digestion model. Journal of Agricultural and Food Chemistry. 2014;62:10055-63.

[36] Chen C, Wang L, Cao F, Miao X, Chen T, Chang Q, Zheng Y. Formulation of 20(S)-protopanaxadiol nanocrystals to improve oral bioavailability and brain

delivery. International Journal of Pharmaceutics. 2016;497:239-47.

[37] Ling J, Yu Y, Zhu J, Li Y, Ling L, Wang L, Xu C, Duan G. A highly sensitive HPLC-MS/MS method for quantification of 20(S)-protopanaxadiol in human plasma and its application in phase IIa clinical trial of a novel antidepressant agent. Journal of Chromatography B. 2016;1031:214-20.

[38] Han E, Lim TG, Kim JE, Yang H, Oh DK, Yoon Park JH, Yoon Park D, Kim HJ, Rhee YK, Lee KW. The ginsenoside derivative 20(S)-protopanaxadiol inhibits solar ultraviolet light-induced matrix metalloproteinase-1 expression. Journal of Cellular Biochemistry. 2017;in press(DOI: 10.1002/jcb.26023).

[39] Jung E, Kang YP, Yoon IS, Kim JS, Kwon SW, Chung SJ, Shim CK, Kim DD. Effect of permeation enhancers on transdermal delivery of fluoxetine: in vitro and in vivo evaluation. International Journal of Pharmaceutics. 2013;456:362-9.

[40] Jung EC, Maibach HI. Animal models for percutaneous absorption. Journal of Applied Toxicology. 2015;35:1-10.

[41] Uchida T, Kadhum WR, Kanai S, Todo H, Oshizaka T, Sugibayashi K. Prediction of skin permeation by chemical compounds using the artificial membrane, Strat-M. European Journal of Pharmaceutical Sciences. 2015;67:113-8.

[42] Karadzovska D, Riviere JE. Assessing vehicle effects on skin absorption using artificial membrane assays. European Journal of Pharmaceutical Sciences. 2013;50:569-76.

[43] Kim JE, Yoon IS, Cho HJ, Kim DH, Choi YH, Kim DD. Emulsion-based colloidal nanosystems for oral delivery of doxorubicin: improved intestinal

paracellular absorption and alleviated cardiotoxicity. International Journal of Pharmaceutices. 2014;464:117–26.

[44] da Silva GB, Scarpa MV, Carlos IZ, Quilles MB, Lia RC, do Egito ES, de Oliveira AG. Oil-in-water biocompatible microemulsion as a carrier for the antitumor drug compound methyl dihydrojasmonate. International Journal of Nanomedicine. 2015;10:585–94.

[45] Silva AE, Barratt G, Cheron M, Egito ES. Development of oil-in-water microemulsions for the oral delivery of amphotericin B. International Journal of Pharmaceutics. 2013;454:641–8.

[46] Aloisio C, Longhi MR, De Oliveira AG. Development and characterization of a biocompatible soybean oil-based microemulsion for the delivery of poorly water-soluble drugs. Journal of Pharmaceutical Sciences. 2015;104:3535–43.

[47] Fricker G, Kromp T, Wendel A, Blume A, Zirkel J, Rebmann H, Setzer C, Quinkert RO, Martin F, Muller-Goymann C. Phospholipids and lipid-based formulations in oral drug delivery. Pharmaceutical Research. 2010;27:1469–86.

[48] Wan T, Xu T, Pan J, Qin M, Pan W, Zhang G, Wu Z, Wu C, Xu Y. Microemulsion based gel for topical dermal delivery of pseudolaric acid B: In vitro and in vivo evaluation. International Journal of Pharmaceutics. 2015;493:111–20.

[49] Chen H, Mou D, Du D, Chang X, Zhu D, Liu J, Xu H, Yang X. Hydrogel-thickened microemulsion for topical administration of drug molecule at an extremely low concentration. International Journal of Pharmaceutics. 2007;341:78–84.

[50] Tamburic S, Craig DQ. The effects of ageing on the rheological, dielectric and mucoadhesive properties of poly(acrylic acid) gel systems. Pharmaceutical Research. 1996;13:279–83.

[51] Islam MT, Rodriguez-Hornedo N, Ciotti S, Ackermann C. Rheological characterization of topical carbomer gels neutralized to different pH. Pharmaceutical Research. 2004;21:1192–9.

[52] Yuan C, Xu Z, Fan M, Liu H, Xie Y, Zhu T. Study on characteristics and harm of surfactants. Journal of Chemical and Pharmaceutical Research. 2014;6:2233–7.

[53] Ohman H, Vahlquist A. In vivo studies concerning a pH gradient in human stratum corneum and upper epidermis. Acta Dermato-Venereologica. 1994;74:375–9.

[54] Mou D, Chen H, Du D, Mao C, Wan J, Xu H, Yang X. Hydrogel-thickened nanoemulsion system for topical delivery of lipophilic drugs. International Journal of Pharmaceutics. 2008;353:270–6.

[55] Chen L, Tan F, Wang J, Liu F. Microemulsion: a novel transdermal delivery system to facilitate skin penetration of indomethacin. Pharmazie. 2012;67:319–23.

[56] Mura P, Faucci MT, Bramanti G, Corti P. Evaluation of transcutol as a clonazepam transdermal permeation enhancer from hydrophilic gel formulations. European Journal of Pharmaceutical Sciences. 2000;9:365–72.

[57] Valenta C, Wanka M, Heidlas J. Evaluation of novel soya-lecithin formulations for dermal use containing ketoprofen as a model drug. Journal of Controlled Release. 2000;63:165–73.

[58] Azzi L, El-Alfy M, Martel C, Labrie F. Gender differences in mouse skin morphology and specific effects of sex steroids and dehydroepiandrosterone. Journal of Investigative Dermatology. 2005;124:22–7.

[59] Rane SS, Anderson BD. What determines drug solubility in lipid vehicles: is it predictable? Advanced Drug Delivery Reviews. 2008;60:638-56.

[60] Ayman El-Kattan and Manthena Varma (2012). Oral absoption, intestinal metabolism and human oral bioavailability, Topics on Durg Metabolism, Dr. James Paxton (Ed.), ISBN: 978-953-51-0099-7, InTech.

[61] Waivor of *in vivo* bioavailability and bioequivalence studies for immediate-release solid oral dosage forms based on a biopharmaceutics calssification system. Guidance for industry. U.S. department of health and human services, Food and drug administration, Center for drug evaluation and research (CDER), U.S. government printing office.

[62] Gursoy RN, Bentina S. Self-emulsifying drug delivery systems (SEDDS) for the improved oral delivery of lipophilic drugs. Biomedicine and Pharmacotherapy. 2004;58:173-82.

[63] Lipinski CA, Lombardo F, Dominy BW, Feeny PJ. Experimental and computational approaches to estimate solubility and permeability in drug discovery and development settings. Advanced Drug Delivery Reviews. 1997;23:3-25.

[64] Tanigawa T, Watanabe T, Ohkawa F, Nadatani Y, Otani K, Machida H, Okazaki H, Yamagami H, Watanabe K, Tominaga K, Fujiwara Y, Takeuchi K, Arakawa T. Rebamipide, a mucoprotective drug, inhibits NSAIDs-induced gastric mucosal injury: possible involvement of the downregulation of 15-

hydroxyprostaglandin dehydrogenase. Journal of Clinical Biochemistry and Nutrition. 2011;48:149-53.

[65] Hong WS, Jung HY, Yang SK, Myung SJ, Kim JH, Min YI, Chung MH, Lee HS, Kim HW. The antioxidant effect of rebamipide on oxygen free radical production by *H. pylori*-activated human neutrophils: in comparison with N-acetylcysteine, ascorbic acid and glutathione. Pharmacological Research. 2001;44:293-7.

[66] Kim CD, Kim HH, Hong KW. Inhibitory effect of rebamipide on the neutrophil adherence stimulated by conditioned media from *Helicobacter pylori*-infected gastric epithelial cells. Journal of Pharmacology and Experimental Therapeutics. 1998;288:133-8.

[67] Tung NT, Park CW, Oh TO, Kim JY, Ha JM, Rhee YS, Park ES. Formulation of solid dispersion of rebamipide evaluated in a rat model for improved bioavailability and efficacy. Journal of Pharmacy and Pharmacology. 2011;63:1539-47.

[68] Pradhan R, Tran TH, Choi JY, Choi IS, Choi HG, Yong CS, Kim JO. Development of a rebamipide solid dispersion system with improved dissolution and oral bioavailability. Archives of Pharmacal Research. 2015;38:522-33.

[69] Guo Y, Wang Y, Xu L. Enhanced bioavailability of rebamipide nanocrystal tablets: formulation and *in vitro*/*in vivo* evaluation. Asian Journal of Pharmaceutical Sciences. 2015;10:223-9.

[70] Bajai A. Rao MR, Khole I, Munjapara G. Self-nanoemulsifying drug delivery system of cefpodoxime proxetil containing tocopherol polyethylene glycol

succinate. Drug Development and Industrial Pharmacy. 2013;39:635-45.

[71] Kim KT, Lee JY, Park JH, Kim MH, Kim JS, Shin HJ, Kang N, Cho HJ, Yoon IS, Kim DD. Development of HPLC method for the determination of buspirone in rat plasma using fluorescence detection and its application to a pharmacokinetic study. Chemical and Pharmaceutical Bulletin. 2016;64:1582-8.

[72] Klossek ML, Marcus J, Touraud D, Kunz W. The extension of microemulsion regions by combining ethanol with other cosurfactants. Colloids and Surfaces A: Physicochemical and Engineering Aspects. 2013;427:95-100.

[73] Yoon IS, Choi MK, Kim JS, Shim CK, Chung SJ, Kim DD. Pharmacokinetics and first-pass elimination of metoprolol in rats: contribution of intestinal first-pass extraction to low bioavailability of metoprolol. Xenobiotica. 2011;41:243-51.

[74] Aungst BJ. Intestinal permeation enhancers. Journal of Pharmaceutical Sciences. 2000;89:429-42.

[75] Shubber S, Vllasaliu D, Rauch C, Jordan F, Illum L, Stolnik S. Mechanism of mucosal permeability enhancement of CriticalSorb® (Solutol® HS 15) investigated *in vitro* in cell cultures. Pharmaceutical Research. 2015;32:516-27.

국문초록

Application of microemulsion for enhancing topical skin absorption of 20(S)-protopanaxadiol and oral

absorption of rebamipide

20(S)-protopanaxadiol (20S-PPD)는 컴파운드 K와 진센노사이드 Rb1 같은 진센노사이드의 당이 떨어진 대사체로서, 강한 피부노화방지 작용을 가진다. 그러나, 20S-PPD의 낮은 수상 용해도와 큰 분자크기 때문에, 이것의 용해도와 피부 투과도를 증진시켜 피부 흡수를 향상시키기 위해서는 적절한 제형화 전략이 필수적이다. Rebamipide (RBP)는 강한 항궤양과 항산화 물질이지만, BCS class IV에 속하는 약물로서, 10%도 안 되는 낮은 경구 생체이용률을 가진다. 그러기에, 경구 적용 후 RBP의 약물학적인 작용이 나타나기 위해서는 RBP의 혈관 순환으로의 전신흡수가 우선적으로 선행되어야 한다. 따라서, 본 연구에서는 20S-PPD의 국소 피부전달과 RBP의 경구전달을 위해서 마이크로에멀젼 기반의 시스템을 개발하고자 하였다. 20S-PPD가 함유된 마이크로에멀젼 및 이를 기반으로 한 하이드로겔 제형들을 만들었으며, 그들의 입자크기 분포, 형태, 최대 로딩 능력, 점도와 pH를 평가하였다. 또한, 헤어리스 마우스 피부 모델과 인공 피부 모델인 스트라트-엠 멤브레인을 이용하여, 최적화된 마이크로에멀젼 기반의 하이드로겔 제형에서의 20S-PPD의 인비트로와 인비보 피부 내 잔류 및 투과 양상을 평가하였다. 20S-PPD를 함유한, 카보폴 중심의 마

이크로에멀젼 기반의 하이드로겔 시스템은 110 nm의 평균 입자 크기와 0.436의 입자크기 분포 지수를 가지며, 성공적으로 만들어졌다. 해당 제형은 최소 56일 동안 안정하였으며, 이것의 점도는 국소 피부로 적용하기에 충분히 높았다. 해당 제형은 헤어리스 마우스 모델에서 20S-PPD의 전신흡수에는 영향을 미치지 않으면서, 20S-PPD의 인비트로 및 인비보 피부 내 잔류를 통계학적으로 유의하게 증가시켰다. 특히, 20S-PPD의 스트라트-엠 멤브레인과 인비트로 및 인비보 헤어리스 마우스 피부 내 잔류 결과에 있어서 시험했던 제형들의 순위가 같았다 (상응계수 r^2 = 0.929-0.947). RBP를 함유한 마이크로에멀젼의 경우, 최대 로딩 능력, 입자크기 분포 및 형태 같은 물성 평가와 인비트로 약물 방출 시험, 인비보 약물동력학 평가 및 소장 독성 시험을 평가하였다. RBP를 함유한, Capmul MCM EP 및 Solutol HS 15 기반의 마이크로에멀젼 시스템은 0.265의 입자크기 분포 지수와 중성의 표면 전하를 가지는 구형의 나노입자(86 nm) 로 이루어졌다. 또한, 해당 마이크로에멀젼은 구별할 만한 소장 독성을 보이지 않은 체로 RBP의 용출과 경구 생체이용률을 통계학적으로 유의하게 증가시켰다. 이들을 종합해보면, 이번 연구에서의 마이크로에멀젼 기반의 제형들은 20S-PPD와 RBP를 포함하는 난용성 물질의 흡수를 증가시키기 위한 효과적인 국소 피부 및 경구 전달 시스템으로서 적

용할 수 있을 것으로 기대되었다.

주요어: 20(S)-protopanaxadiol (20S-PPD); rebamipide (RBP); microemulsion (ME)-based systems; topical skin delivery; oral delivery; poorly soluble compound

학번: 2011-21702

Appendix